Revealing trap depth distributions in persistent phosphors with a thermal barrier for charging

Ang Feng,[1, 2] Jonas J. Joos,[1, 2] Jiaren Du,[1, 2, 3] and Philippe F. Smet[1, 2, *]

[1]*LumiLab, Department of Solid State Sciences, Faculty of Sciences,*
Ghent University, Krijgslaan 281-S1, Gent 9000, Belgium
[2]*Center for Nano- and Biophotonics (NB-Photonics), Ghent University, Belgium*
[3]*International Joint Research Center for Photo-responsive Molecules and Materials,*
School of Chemical and Material Engineering, Jiangnan University, Wuxi 214122, China

(Dated: November 16, 2021)

The performance of persistent phosphors under given charging and working condition is determined by the properties of the traps that are responsible for these unique properties. Traps are characterized by the depth of their associated thermal barrier and a continuous distribution of trap depths is often found in real materials. Accurately determining trap depth distributions is hence of importance for the understanding and development of persistent phosphors. However, extracting the trap depth distribution is often hindered by the presence of a thermal barrier for charging, which causes a temperature-dependent filling of traps. For this case, we propose a method for extracting the trap depth distribution in this case from a set thermoluminescence glow curves obtained for variable charging temperature. The glow curves are transformed into electron population functions via the Tikhonov regularization in the framework of first-order kinetics. Subsequently, the evolution of the occupation of the traps as a function of trap depth, quantified by the so-called filling function, is obtained. Finally, the underlying trap depth distribution can be reconstructed by two proposed methods. The proposed method provides good precision and resolution for the trap depth distribution, which is a step forward in acquiring a deeper understanding of the (de)trapping behavior of persistent and storage phosphors.

I. INTRODUCTION

It is a materials scientist's dream to tailor materials properties by tuning only a few intrinsic parameters of the materials. This is true for persistent phosphors whose luminescence persists from seconds to days after stopping the optical excitation (i.e., charging) [1–4]. High persistent luminescence (PersL) intensity and long PersL duration are two desirable properties under given charging and working conditions [5]. One critical parameter controlling these properties is the density of traps, i.e., the absolute number of active traps per unit volume of the persistent phosphor. The higher the trap density, the more electrons a phosphor can store at the given charging condition, enhancing PersL intensity. Electrons are considered as the common charge carriers, although holes can act as the charge carriers in certain cases [3, 6]. Another parameter is the distribution of trap density with respect to trap depth E_t, which quantifies the energy barrier that trapped electrons must overcome to recombine with holes. It is usually called trap depth distribution for short, being denoted as $N(E_t)$. These parameters are scientifically important. At one hand, they are useful to understand and thus to tailor performances of persistent phosphors under different conditions. For example, the trap depth distribution can be translated into thermoluminescence (TL) profiles, which show a linear relationship with respect to the integrated PersL intensity for a

given charging and working temperature [7, 8]. This suggests a subtle relationship between trap depth distribution and the optimum working temperature of persistent phosphors. On the other hand, such parameters act as intrinsic materials parameters that can be compared across different phosphors, enabling the discovery of empirical rules in persistent phosphors. This is particularly useful for materials discovery via machine learning [9], where intrinsic materials parameters add reliable 'features'.

There are multiple difficulties when it comes to extracting the trap density and trap depth distribution. After charging ($t = 0$), the density of trapped electrons (called here the electron population function) $n(E_t, q, t)$ is determined by the trap depth distribution $N(E_t)$ and the filling function $f(E_t, \Delta E, q, t)$ via,

$$n(E_t, q, t) = f(E_t, \Delta E, q, t)N(E_t) \quad (1)$$

where the charging parameter vector $q = [I_e(\lambda), t_{ch}, T_{ch}]$ includes the irradiance $I_e(\lambda)$, the charging duration t_{ch} and the charging temperature T_{ch}, i.e. all experimentally accessible settings. In the trap depth range $[E_t, E_t+dE_t]$, the filling function $f(E_t, \Delta E, q, t)dE_t$ indicates the fraction of the traps that are filled at time t after charging with parameter vector q. In Eq. 1, ΔE is the thermal barrier for charging, which renders the maximum of the filling function dependent on charging temperature (with $I_e(\lambda)$ and t_{ch}). This phenomenon has been observed in many persistent phosphors, for example $SrAl_2O_4$:Eu^{2+} [10], $Sr_2MgSi_2O_7$:Eu^{2+} [11], $M_2Si_5N_8$:Eu (M = Ca, Sr, Ba) [12], $Y_3Al_5O_{12}$:Ce^{3+} [13],$Y_3Al_{5-x}Ga_xO_{12}$:Pr^{3+} [14] and other garnets [15–18]. The thermal barrier severely complicates the extraction of trap depth distributions

* Philippe.Smet@UGent.be

from experiments.

The first obstacle is to recover the electron population function $n(E_t, q, t)$ from experimental TL curves. In current literature, methods are proposed to approximate the trap depth distribution by the electron population function, assuming that traps can be fully filled at the given charging condition. The simplest approximation of the electron population function is a delta function $N_0\delta(E_t - E_o)$, which can be characterized by a characteristic trap depth E_o and the total number of traps per volume N_0. The quantity N_0 can be calculated by the method proposed by Van der Heggen et al [19]. The discrete trap depth E_o can be estimated by several methods [20, 21], such as the initial rise method [22, 23], the Urbach relation [24], and the analysis of position and symmetry of the glow curve [20, 21]. Advanced methods are proposed to infer $n(E_t, q, t)$ for which traps are assumed to be distributed with respect to the trap depth. For example, the fractional glow technique [25, 26] and the T_m-T_{stop} method [23, 27] approximate $n(E_t, q, t)$ by providing the trapped electrons in certain trap depth ranges which are accessed by the specially designed heating procedures. Recently, V. M. Khanin proposed to recover $n(E_t, q, t)$ from a TL curve directly by numerical regularization method, assuming first-order kinetics is valid for TL [28].

The main difficulty of extracting the full trap depth distribution $N(E_t)$ lies in approximating the filling function after charging $f(E_t, \Delta E, q, t)$, especially when there exists a thermal barrier for charging ΔE. At a given charging temperature T_{ch}, $f(E_t, \Delta E, q, t = 0)$ approaches the Fermi-Dirac function in the limit of $t_{ch} \rightarrow \infty$ [29],

$$f(E_t, \Delta E, q, t = 0) = \frac{f_0(\Delta E, q)}{1 + \exp\left(-\frac{E_t - E_f}{k_{\mathrm{B}}T_{ch}}\right)} \quad (2)$$

where k_{B} is the Boltzmann constant, E_f the quasi-Fermi level and $f_0(\Delta E, q)$ the magnitude of the filling function. $f_0(\Delta E, q)$ is less than 1.0 because of various detrapping routes, such as thermal detrapping and optically stimulated detrapping [11, 30]. To access a wide range of E_f, phosphors are often charged at variable temperature T_{ch} with fixed irradiance I_e and fixed duration t_{ch}. When a thermal barrier ΔE is absent, $f_0(\Delta E, q)$ is independent of T_{ch}. The trap depth distribution in a range of $[E_f(T_{ch}), E_f(T_{ch} + \Delta T_{ch})]$ can be approximated by the difference of the total number of trapped electrons [31]. Experimentally, this can be determined from the difference in the integrated intensity of TL glow curves obtained at variable charging temperature T_{ch}. However, the thermal barrier ΔE poses two challenges for extracting the trap depth distribution $N(E_t)$. One is to approximate $f_0(\Delta E, q)$ for each filling function at charging temperature T_{ch}. The other is to reconstruct the trap depth distribution $N(E_t)$ from various individual pairs of $f(E_t, \Delta E, q, t)$ and $n(E_t, q, t)$. It is noteworthy that the thermal barrier ΔE is treated as an empirical
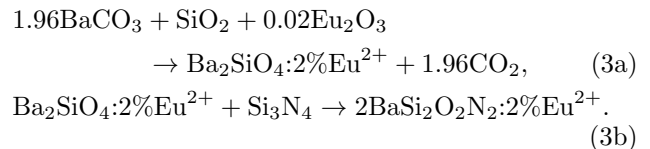
parameter to account for the temperature dependence of $f_0(\Delta E, q)$. It is different from the activation energy of thermal quenching, which often originates from the cross-over of potential curves due to electron-phonon interaction [32] or the thermal ionization of the electrons at the excited states of the involved luminescent centers (e.g. Ce^{3+} or Eu^{2+}) [33, 34].

In this work, we propose a method that circumvents the influence of ΔE and allows to extract the trap depth distribution $N(E_t)$ from TL experiments. The phosphor $BaSi_2O_2N_2$:2%Eu^{2+} was used as a model to validate the proposed method. In addition to desirable properties such as PersL [35] and mechanoluminescence [36–38], this phosphor shows a high photoluminescence quantum efficiency and great thermal stability [39], enabling high TL signal strength at elevated temperatures. The phosphor was charged at variable temperature T_{ch} with fixed irradiance I_e and fixed duration t_{ch}, and thermoluminescence glow curves were collected accordingly (see Fig. 1). First-order kinetics is hypothesized here within a framework of local electron trapping and recombination. This was supported by various experimental and theoretical results on similar phosphors [10, 11, 40–42]. The electron population function $n(E_t, q, t)$ will be inferred from experimental TL curves via the Tikhonov regularization method. According to the simulation of the charging kinetics, a method was proposed to estimate the magnitude of the filling function $f_0(\Delta E, q)$ from $n(E_t, q, t)$. Subsequently, two approaches can be adopted to reconstruct the trap depth distribution from filling functions and the electron population functions.

The method is extendable to other materials when the trap depth distribution can be translated into TL. Accurate determination of the trap depth distribution will lead to a step forward in understanding the properties of persistent and storage phosphors.

II. MATERIALS AND METHODS

The $BaSi_2O_2N_2$:2%Eu^{2+} phosphor was prepared by a two-step solid-state reaction method [43], according to:

$$1.96BaCO_3 + SiO_2 + 0.02Eu_2O_3$$
$$\rightarrow Ba_2SiO_4\text{:2\%}Eu^{2+} + 1.96CO_2, \quad (3a)$$
$$Ba_2SiO_4\text{:2\%}Eu^{2+} + Si_3N_4 \rightarrow 2BaSi_2O_2N_2\text{:2\%}Eu^{2+}. \quad (3b)$$

The raw materials $BaCO_3$ (99.8 %, 1 μm powder, Alfa Aesar), SiO_2 (99.5%, 325 mesh powder, Alfa Aesar), and Eu_2O_3 (99.9%, Alfa Aesar) were used in stoichiometric amount except that 103% Si_3N_4 (α phase, 99.9%, 1 μm powder, Alfa Aesar) was supplied to facilitate the reduction of Eu^{3+} to Eu^{2+} [44]. The sintering temperature and duration for Eq. 3a and Eq. 3b were 1200 °C, 4 h and 1450 °C, 10 h, respectively. A 94% N_2-6% H_2 forming gas was applied at a constant rate (0.16 L/min) during the entire thermal process. The product was crushed and
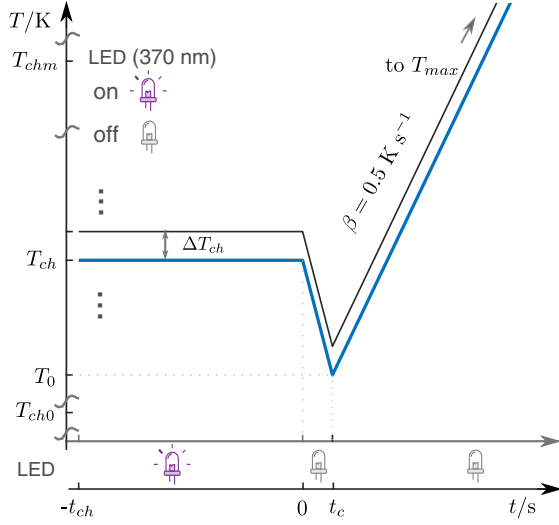
FIG. 1. **The procedure for a TL experiment**. The phosphor was charged by UV light and fixed a charging duration t_{ch} at variable charging temperature T_{ch}. After lowering the temperature to $T_0 \leq T_{ch} - 30K$, the phosphor will be heated to temperature T_{max} with fixed heating rate β (0.5 K s^{-1}). Here, $T_{ch} = [T_{ch0} : \Delta T_{ch} : T_{chm}]$, with $\Delta T_{ch} = 5$ K, $T_{ch0} = 223$ K, and $T_{chm} = 393$ K.

ground to fine powders, and then washed by diluted hydrogen chloride (HCl,<1 vol%). After being dried at 80 °C for at least 10 h, BaSi$_2$O$_2$N$_2$:2%Eu^{2+} powders were finally ready for further use.

A thermal quenching (TQ) profile was collected to correct TL curves by using the method proposed in Ref [45]. The spectra were acquired at a home-built setup which is capable of providing wavelength resolution at both excitation and detection sides [10]. The excitation light of 370 nm (full-width-half-maximum (fwhm) 5 nm) was from a Xe arc lamp equipped with a monochromator, while the emission was collected by an EMCCD camera (Princeton Instruments ProEM 1600) coupled to a spectrograph (Princeton Instruments Acton SP2300). The integration time was 1 s. The phosphor was cooled to 213 K and then heated to 498 K at a step of 5 K, with optical excitation at each temperature T for 30 s. For each T, five spectra from the time range from 24 to 28 s were averaged to represent the PL emission intensity $I(T)$ (Supplemental material (SM) [46], section I). For each TL curve, the measured TQ was linearly interpolated at each temperature recording of the TL curve.

The procedure for extracting trap depth distribution characterizes fixed irradiance, fixed charging duration, and variable charging temperature T_{ch} (Fig. 1). The UV light (370 nm, fwhm 20 nm) was from an light-emitting-diode (LED) which was driven by a current J of 50 mA and the charging duration was set to 300 s. The charging temperature was set in the range $T_{ch} = [T_{ch0} : \Delta T_{ch} : T_{chm}]$, with $\Delta T_{ch} = 5$ K, $T_{ch0} = 223$ K, and $T_{chm} = 393$ K. To acquire a TL curve, the phosphor was first excited at T_{ch} for 300 s and then cooled down at a rate
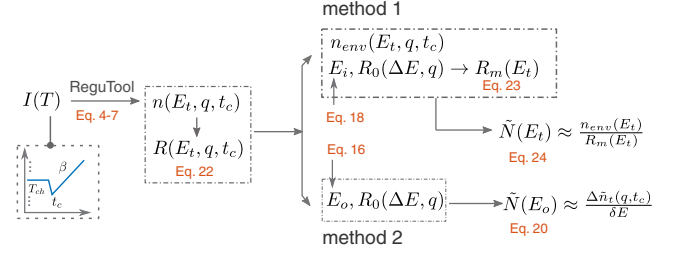

FIG. 2. **Flowchart of the method**. The TL curves are first converted into electron population functions, and the relative filling functions are approximated. Two methods can be chosen to calculate the trap depth distribution $N(E_t)$.

of 0.5 K/s to T_0 ($T_0 \leq T_{ch} - 30$ K), where the TL intensity is negligible. Finally, the phosphor was heated up to 493 K at the heating rate $\beta = 0.5$ K/s. The emission was detected by a photometer (International Light Technologies, ILT1700) equipped with a photopic filter (YPM). Every TL curve was corrected by a TQ profile to remedy the non-radiative transition of the luminescent centers.

III. RESULTS

We briefly outline the procedure of extracting a trap depth distribution (see Fig. 2), which is the focus of the following sections. In section III A, the electron population functions $n(E_t, T_{ch}, t_c)$ are reconstructed from the experimental TL curves from a carefully designed charging procedure (see section II). A numerical recipe called the Tikhonov regularization method within the framework of first-order kinetics of TL is used to solve this inverse problem (see Equations (S3) to (5) and (7)). The presence of a thermal barrier ΔE can be inferred from these electron population functions. In section III B, first-order kinetics for trapping and recombination during charging process is proposed to calculate the filling function (Eq. 21). From the simulation, a method is proposed to approximate the magnitude of the filling function $f_0(\Delta E, q)$. The subtle relationship between the pair of $f_0(\Delta E, q)$ and $n(E_t, q, t)$ and the trap depth distribution $N(E_t)$ can be revealed accordingly. In section III C, the trap depth distribution of BaSi$_2$O$_2$N$_2$:2%Eu^{2+} will be reconstructed by two approaches to validate the proposed method. These approaches reach consistent results.

A. Electron population function

Thermoluminescence (TL) was chosen to infer the electron population functions after charging because of the clear physics picture and convenience of implementation. First-order kinetics is assumed for TL and retrapping of electrons among traps is the main process that leads to non-first order kinetics. During a TL experiment, re-

trapping usually does not play a dominant role because the rate coefficient of detrapping increases substantially with increasing temperature. Assuming first-order kinetics thus leads to a convenient means to infer the information of a phosphor during/after charging.

1. Tikhonov regularization method

According to the first order kinetics, the TL intensity from an electron population function $n(E_t, q, t_c)$ is given by the Fredholm integral of the first kind [47, 48],

$$I(T) = C \times \int_0^\infty n(E_t, q, t_c) K(E_t, T) dE_t, \qquad (4a)$$

$$K(E_t, T) = \frac{\nu_r}{\beta} \exp\left[-\frac{E_t}{k_B T} - F(E_t, T) + F(E_t, T_0) \right], \qquad (4b)$$

$$F(E_t, T) = \frac{\nu_r}{\beta} \int_0^T \exp\left(-\frac{E_t}{k_B T'} \right) dT', \qquad (4c)$$

where the function $K(E_t, T)$ is referred to as the kernel that translates the electron population function $n(E_t, q, t_c)$ to the TL intensity $I(T)$ and $F(E_t, T)$ is often called the temperature integral [49]. In Eq. 4, C a coefficient to render the appropriate units for $I(T)$ and the meanings of $t_c, T_0,$ and β have been elucidated in Section II (see Fig. 1). Eq. 4a was proposed by Randall and Willkins [50, 51] early in 1945, but the electron population function $n(E_t, q, t_c)$ was replaced by a trap depth distribution $N(E_t)$.

An analytic expression for $F(E_t, T)$ was proposed by M. Balarin [52],

$$F(E_t, T) = \frac{\nu_r}{\beta} \frac{k_B T^2}{E_t} \exp\left(-\frac{E_t}{k_B T} \right) \frac{1}{\sqrt{1 + 4k_B T/E_t}}, \quad (5)$$

which offers high accuracy even when $E_t/k_B T$ is small [53]. This analytic formula removes the technical difficulties in computing the kernel.

The electron population function $n(E_t, q, t_c)$ can be numerically obtained by solving Eq. 4 with the formula Eq. 5. As a first step, the temperature and energies are discretized over a grid $[T_0, T_m] \times [E_a, E_b]$,

$$Kn = I, \qquad (6)$$

which is equivalent to Eq. 4a. Herein, K, I and n are matrices representing the kernel, experimental TL data and electron population function, respectively. The integral equation Eq. 4 and its discrete counterpart Eq. S3 are ill-conditioned and the approximated solutions are possible under the Picard condition [54]. Therefore, no stable solution for n can be extracted from Eq. S3 by linear least square methods, i.e., seeking $\hat{n}$ that minimizes the residual norm squared $\|K\hat{n} - I\|_2^2$. The Tikhonov regularization method can solve this inverse problem by minimizing the functional [55, 56],

$$V(\hat{n}) = \|K\hat{n} - I\|_2^2 + \lambda^2 \|L\hat{n}\|_2^2 \qquad (7)$$
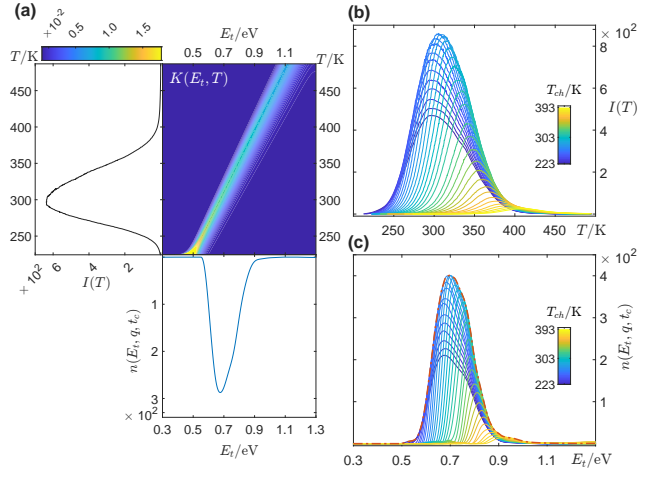

FIG. 3. **The electron population function** $n(E_t, q, t_c)$. **(a)** The kernel $K(E_t, T)$ maps the TL curve $I(T)$ into the electron population function $n(E_t, q, t_c)$ via discrete regularization method Eq. 4 ($T_{ch} = 243$ K). For variable charging temperature T_{ch}, the TL curves **(b)** can thus turn into the electron population functions $n(E_t, q, t_c)$ **(c)**, from which an envelope can be constructed accordingly (the orange line). Note $\nu_r = 10^{10}$ Hz.

in which λ is the regularization parameter, and L is the discrete approximation of a derivative operator. Additionally, non-negativity constraint is imposed for the solution, i.e. $\hat{n} \geq 0$. This regularization operator favors smooth solutions for $\hat{n}$ (small derivatives), leading to an improved numerical stability of the solution. The smoothness of $\hat{n}$ is hence implicitly assumed during Tikhonov regularization, and agrees with the physical picture of electron population functions. The value of λ fixes the relative weights of both contributions in the minimization and is numerically chosen to guarantee a good balance between regularization and agreement to experiment [57]. In this work, the Tikhonov regularization is implemented via the *Regularization Tools* MATLAB package [58, 59]. More details are given in section II of SM [46].

The kernel $K(E_t, T)$ maps TL curves into electron population functions via the Tikhonov regularization method. An individual example is shown in Fig. 3a, for which $T_{ch} = 243$ K. TL curves and the electron population functions are displayed in Fig. 3b and Fig. 3c for $T_{ch} = [T_{ch0} : \Delta T_{ch} : T_{chm}]$, with $\Delta T_{ch} = 5$ K, $T_{ch0} = 223$ K, and $T_{chm} = 393$ K. Obviously, the higher the T_{ch} the higher the tails of electron population functions, suggesting that a temperature dependent filling of traps. Furthermore, an envelope of the electron population functions, i.e. $n_{env}(E_t, q, t_c)$, can be calculated by an interpolation method (section III of SM [46]). Shown as the orange line in Fig. 3c, the envelope $n_{env}(E_t, q, t_c)$ will be crucial to reconstruct high-precision trap depth distribution, which will be discussed in section III B.
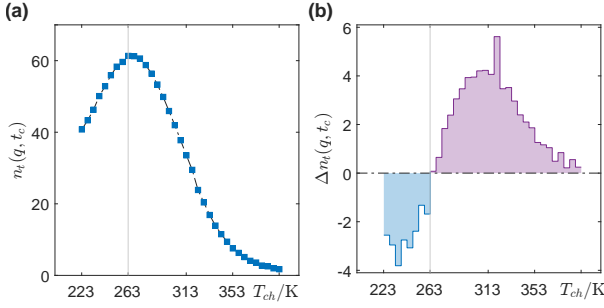
FIG. 4. **The presence of ΔE. (a)** The total number of trapped electrons per volume $n_t(q, t_c)$ as a function of T_{ch} reaches a peak at $T_{ch} \approx 263$ K. **(b)** As T_{ch} decreases, the corresponding difference $\Delta n_t(q, t_c)$ turns from positive into negative at $T_{ch} \approx 263$ K.

2. The presence of a thermal barrier

The presence of a thermal barrier for charging can be revealed qualitatively. For each electron population function $n(E_t, q, t_c)$, the total number of trapped electrons per volume can be calculated accordingly,

$$n_t(q, t_c) = \int_{E_a}^{E_b} n(E_t, q, t_c) dE_t, \tag{8}$$

and the corresponding difference $\Delta n_t(q, t_c)$ can be calculated as,

$$\Delta n_t(q, t_c) = n_t(q_1, t_c) - n_t(q, t_c). \tag{9}$$

Herein, $q \to T_{ch}$ means q can be represented by T_{ch} since I_e and t_{ch} are already fixed, and the same representation rule applies for $q_1 \to T_{ch} - \Delta T_{ch}$ as well.

When $\Delta E = 0.0$ eV (i.e., in the absence of a thermal barrier for charging), $n_t(q, t_c)$ should be a non-decreasing function with decreasing T_{ch} because more shallow traps can be filled at lower temperature. To put it another way, the corresponding difference $\Delta n_t(q, t_c)$ will always be non-negative. This is not the case for the phosphor under study, as shown in Fig. 4. At $T_{ch} \approx 263$ K, $\Delta n_t(q, t_c)$ turns from positive to negative, which means the traps are already less efficiently filled as T_{ch} decreases. This suggest the presence of a thermal barrier for charging.

B. Filling function

The kinetics of electron transitions in charging processes is required to reveal information of the filling function after charging. Such information provides a guideline to interpret the electron population function and to calculate the filling function. In this section, the trapping and recombination processes are assumed to take place within isolated pairs and thus first-order kinetics is hypothesized naturally (section III B 1). Given appropriate parameters, the filling function can be simulated under the proposed charging procedure. The method of extracting the filling function is revealed from the simulation, and two methods of reconstructing trap depth distribution are proposed accordingly (section III B 2).

1. Local transition

It is typically reckoned that two different species are involved in persistent luminescence and thermoluminescence processes: the luminescence centers and the traps. A luminescent center, e.g. Eu^{2+}, has a ground state and a dense manifold of excited states [60]. In the models for the dynamics in TL, the complex ground and excited state electronic structures are typically regarded in a mean-field single-electron approximation, leading to few orbitals that a charge carrier can occupy or not [48]. As such, a luminescent center is usually approximated by one ground state and one excited state, leading to a four-orbital energy level scheme for which equilibrium occupations can be modeled via the Fermi-Dirac distribution. An electron in the excited orbital of the luminescent center either decays radiatively to the ground state of the luminescent center or gets trapped at a trap if it is able to overcome the thermal barrier ΔE (Fig. 5a). Chemically, a trap can be a lattice defect, e.g. an oxygen vacancy [61] or even a co-dopant, like the case of Dy in $Sr_4Al_{14}O_{25}$: Eu^{2+},Dy^{3+} [62]. If an electron trap is empty, it can capture an electron. If the trap is filled, it can supply an electron to recombine with a hole nearby, provided that the electron can overcome the thermal barrier E_t, .i.e. the trap depth (Fig. 5b). This detrapping process is referred to as recombination. The hole in persistent phosphor is often reckoned as immobile since its mobility is much smaller than that of electrons. In case of Eu^{2+}-based persistent phosphors, the hole is localized at the (photo-)oxidized Eu^{2+}, i.e. the Eu^{3+} center. In the remainder, the situation where an electron in a filled trap is transferred to recombine with a (localized) hole is referred to as an electron-hole pair. Furthermore, the process where an electron is transferred from a filled trap to another empty trap, i.e. retrapping, is not considered.

Assuming first-order kinetics in the local transition model is very reasonable. At one hand, the density of luminescent centers (usually of the order of 1 mol%) is often greater than that of empty traps when they are crystallographic defects, making that luminescent-center-trap pairs are far apart. On the other hand, empty traps can only be filled to a limited level by exciting the luminescent centers, even if the density of traps is high, as is the case of Dy in $Sr_4Al_{14}O_{25}$:Eu^{2+},Dy^{3+} [62], making that electron-hole pairs are thus far apart. Therefore, first order kinetics emerge naturally since the involved pairs are isolated and independent. An isolated luminescent-center-trap pair can only transform into an electron-hole pair upon trapping, while the electron-hole pair turns into a luminescent center and an empty trap upon recombination. Here, it is assumed that the charge trans-
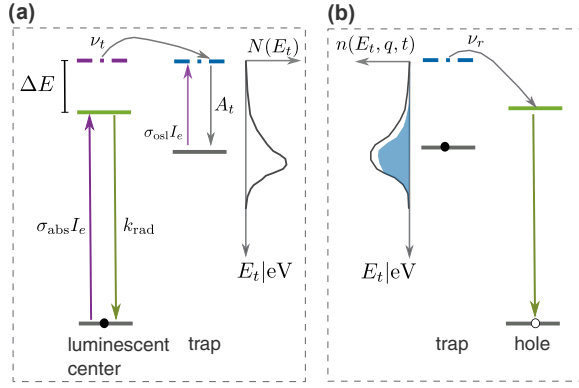
FIG. 5. **Local model for trapping and recombination**. The isolated pairs approximation is assumed for trapping and recombination. **(a)** The trapping process takes place within a pair of luminescent center and an empty trap, i.e. a luminescent-center-trap pair. **(b)** Recombination takes place with a pair of filled trap and a hole, i.e. an electron-hole pair. Parameters are displayed for important electron transitions. The trap depth distribution $N(E_t)$ and electron population function $n(E_t, q, t_c)$ are shown as gray curve and blue filled area, respectively.

fer dominantly takes place within pairs with the shortest separation , i.e., the nearest neighbor assumption (NNA). Under this assumption, the density of electron-hole pairs is proportional to the density of filled traps [63]. Therefore, the filling function $f(E_t, \Delta E, q, t)$ itself follows the first-order ordinary differential equation,

$$\frac{\partial f(E_t, \Delta E, q, t)}{\partial t} = k_{\text{trap}}(\Delta E, q) \left[1 - f(E_t, \Delta E, q, t)\right]$$
$$- k_{\text{rcb}}(E_t, q) f(E_t, \Delta E, q, t), \quad (10)$$

where $k_{\text{trap}}(\Delta E, q)$ and $k_{\text{rcb}}(E_t, q)$ are the trapping coefficient and recombination coefficient, respectively.

The trapping and recombination coefficients in Eq. 10 can be deduced by analyzing the kinetics of elementary trapping and recombination events. At the time scale needed to register an TL data (often > 10 ms), the density of electrons in the excited state of a luminescent or a trap will have reached its maximum change upon any abrupt perturbation. The trappping and recombination coefficients can thus be approximated by analyzing the relative values of the coefficients associated in trapping and recombination (depicted in Fig. 5), respectively. According to the analysis in section IV of SM [46], the trapping and recombination coefficients read,

$$k_{\text{trap}}(\Delta E, q) = \nu_t \exp\left(-\frac{\Delta E}{k_{\text{B}} T}\right) \frac{\sigma_{\text{abs}} I_e(\lambda)}{k_{\text{rad}}}, \quad (11)$$

$$k_{\text{rcb}}(E_t, q) = \frac{A_t}{A_t + \nu_r} \left[\nu_r \exp\left(-\frac{E_t}{k_{\text{B}} T}\right) + \frac{\nu_r}{A_t} \sigma_{\text{osl}} I_e(\lambda)\right], \quad (12)$$

respectively. Here σ_{abs} is the optical absorption cross section of Eu^{2+}, and k_{rad} is the spontaneous emission

TABLE I. The parameters for simulations

Parameter	Unit	Value	Comment
ΔE	eV	0.255	
σ_{abs}	cm^2	3×10^{-18}	
σ_{osl}	cm^2	10^{-17}	
k_{rad}	MHz	1.54	see Ref. [39]
ν_r	Hz	10^{10}	
ν_t	Hz	10^{10}	
A_t	Hz	10^{12}	
$I_e(\lambda)$	$\frac{\text{photons}}{cm^2 s}$	5×10^{15}	$\lambda = 370$ nm [a]
T_{ch}	K	-	[b]
t_{ch}	s	-	
k_{B}	eV K^{-1}	8.617×10^{-5}	

[a] The values are specified in the figures or their captions.
[b] The values are specified in the figures or their captions.

coefficient of the 5d orbital of Eu^{2+}. Similarly for traps, σ_{osl} is the absorption cross section of optically stimulated detrapping, while A_t is the de-excitation coefficient of the excited orbital of the trap, regardless of its depth. The frequency factors ν_r and ν_t represent the trapping and recombination processes, respectively.

For a phosphor with all traps initially empty, an optical charging with fixed irradiance $I_e(\lambda)$, duration t_{ch} and temperature T_{ch} leads to the filling function as a solution of Eq. 10,

$$f(E_t, \Delta E, q, t = 0) = \frac{k_{\text{trap}}(\Delta E, q)}{k_{\text{trap}}(\Delta E, q) + k_{\text{rcb}}(E_t, q)}$$
$$\times \left\{1 - \exp\left[-\left(k_{\text{trap}}(\Delta E, q) + k_{\text{rcb}}(E_t, q)\right) t_{ch}\right]\right\}. \quad (13)$$

Clearly, the magnitude and shape of the filling function are influenced by the thermal barrier ΔE. The cooling after charging (see Fig. 1) further reduces the filling function to

$$f(E_t, \Delta E, q, t_c) = f(E_t, \Delta E, q, t = 0)$$
$$\times \exp\left[-F(E_t, T_0) + F(E_t, T_{ch})\right]. \quad (14)$$

It is unrealistic to fit this model directly to experimental observations because there is a huge number of parameters, many of which are not easily available. Instead, parameters are provided from experimental findings or estimation which gives values in a reasonable range, as shown in Table I. For example, the thermal barrier for charging ΔE takes an arbitrary value of 0.255 eV. Actually, the exact value of ΔE is not so important because it dominantly influences the magnitudes of filling functions, which can be corrected in certain ways. The simulation of filling function Eq. 13 and Eq. 14 is conducted to analyze the filling function under the designed charging procedure. From the analysis, methods of extracting trap depth distribution will be proposed in the coming sections.
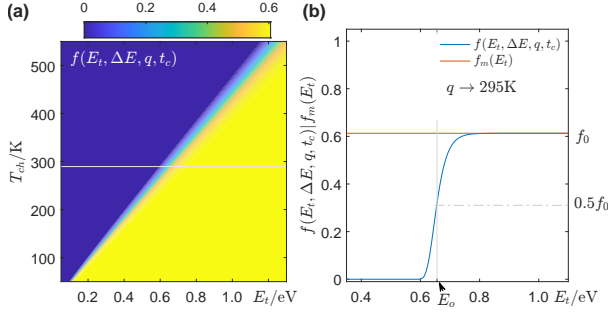
FIG. 6. **The filling function in the case without a thermal barrier for charging ($\Delta E = 0.0$ eV). (a)** The contour plot of the filling function $f(E_t, \Delta E, q, t_c)$ in the $T_{ch} \times E_t$ plane ($q \to T_{ch}$). The gray line indicates the filling function for $q \to 295$ K. **(b)** The magnitude of filling $f_m(E_t)$ is independent of charging temperature T_{ch}. An individual filling function, e.g. that for $q \to$295 K, characterizes a magnitude of filling f_0 and a characteristic trap depth E_o. Note that $T_0 = T_{ch} - 40$ K and $t_{ch} = 0.01$ s.

2. Analysis of filling functions

By using parameters in Table I, the filling function $f(E_t, \Delta E, q, t_c)$ (Eq. 14) was simulated at variable charging temperature T_{ch}, with fixed charging duration t_{ch}, fixed charging irradiance I_e, and $T_0 = T_{ch} - 40$ K (cooling rate 1.0 K s^{-1}). The filling functions for $\Delta E = 0.0$ eV and $\Delta E = 0.255$ eV are discussed in the following to reveal the methods of extracting trap depth distributions.

$\Delta E = 0.0$ **eV**. In this case, the magnitudes of filling functions are independent of charging temperature T_{ch}. The contour plot of $f(E_t, \Delta E, q, t_c)$ in the $T_{ch} \times E_t$ plane is shown in Fig. 6a, where the filling function for $q \to$ 295 K is indicated by the gray line. As shown in Fig. 6b, an individual filling function can be characterized by its magnitude f_0 and an characteristic trap depth E_o. The filling function can be approximated by a Heaviside step function, i.e.,

$$f(E_t, \Delta E, q, t_c) \approx f_0(\Delta E, q) H[E_t - E_o(q)], \quad (15)$$

where E_o is determined by the relation accordingly,

$$f(E_o, \Delta E, q, t_c) = 0.5 f_0(\Delta E, q). \quad (16)$$

Therefore, the pair of E_o and $f_0(\Delta, q)$ represents the corresponding filling function under the charging condition q. After taking all filling functions into account, a function $f_m(E_t)$ that characterize the magnitude of the filling function under variable charging temperature ($q \to T_{ch}$) can be defined,

$$f_m(E_t) : E_t(q) \mapsto f_0(\Delta E, q), \quad (17)$$

which fully account for the influence of ΔE on the magnitude of filling function. Hence, $f_m(E_t)$ is called the magnitude function. From Fig. 6b, the magnitude function $f_m(E_t)$ (orange line) is independent of E_t and thus of charging temperature T_{ch}.
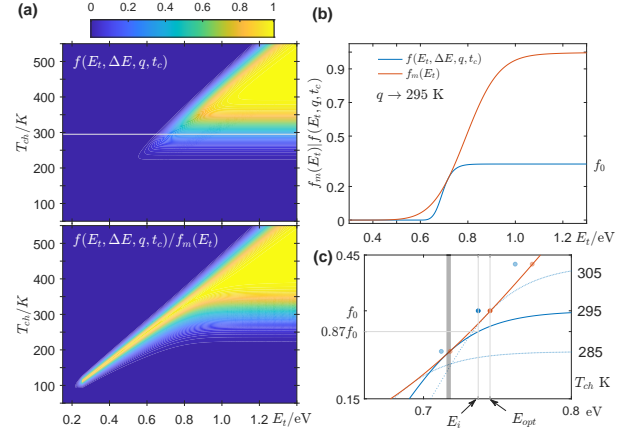

FIG. 7. **The filling function in the case of a thermal barrier for charging ($\Delta E = 0.255$ eV). (a)** The contour plots of filling function $f(E_t, \Delta E, q, t_c)$ (top panel) and normalized filling function $f(E_t, \Delta E, q, t_c)/f_m(E_t)$ (bottom panel) in the $T_{ch} \times E_t$ plane ($q \to T_{ch}$). **(b)** The magnitude function $f_m(E_t)$ is tangent to the filling function $f(E_t, \Delta E, q, t_c)$. **(c)** The magnitude function $f_m(E_t)$ can be approximated by the characteristic trap depth E_i and the magnitude $f_0(\Delta E, q)$ of the filling function.

A method of extracting trap depth distributions becomes visible in this case. Given the charging condition $q \to T_{ch}$ and $q_1 \to T_{ch} - \Delta T_{ch}$, the difference of the total number of traps per volume $\Delta n_t(q, t_c)$ (Eq. 9) is proportional to $N(E_t)$ for $E_t \in [E_t(q_1), E_t(q)]$. No correction is needed for either the magnitude $f_m(E_t)$ or the electron population function $n(E_t, \Delta E, q, t_c)$. This is the essence of the method from Ref. [31], in which E_o is extracted by the initial rise method. The current method performs better than that in [31] in terms of clear physics picture and precision of extracting E_o.

Non-zero ΔE. The filling function with non-zero ΔE clearly indicates the dependence of the magnitude function $f_m(E_t)$ on the charging temperature T_{ch}. The contour plot for $f(E_t, \Delta E, q, t_c)$ with $\Delta E = 0.255$ eV (Fig. 7a, top panel) shows that the filling of traps depends on the charging temperature T_{ch}. Every filling function $f(E_t, \Delta E, q, t_c)$ can be normalized by its magnitude $f_0(\Delta E, q)$, and the contour plot of the normalized filling function is presented in Fig. 7a as $f(E_t, \Delta E, q, t_c)/f_m(E_t)$ (bottom panel). For a given range of trap depths, there exists an optimal charging temperature range that optimizes the output of persistent luminescence, which has been observed in many phosphors [7]. The magnitude function $f_m(E_t)$ (Fig. 7b), which is tangent to the filling functions, shows an increasing function with increasing trap depth, indicating the presence of a thermal barrier for charging ΔE.

The magnitude function $f_m(E_t)$ carries two important implications, which are crucial for the extraction of trap depth distributions. One is that it can be approximated from filling functions, which is illustrated in Fig. 7c. For a given filling function $f(E_t, \Delta E, q, t_c)$, the magnitude

$f_0(\Delta E, q)$ can be easily extracted and it corresponds to a theoretical trap depth E_{opt} which satisfies,

$$f_m(E_{opt}) = f_0(\Delta E, q).$$

However, E_{opt} is inaccessible experimentally because the magnitude function, which is the heavily sought after, is unknown beforehand. By using the filling function alone, a characteristic trap depth E_i is used to approximate the theoretical E_{opt} according to the relation,

$$f(E_i, \Delta E, q, t_c) = 0.87 f_0(\Delta E, q). \tag{18}$$

Here, the scalar 0.87 is an empirical constant. For a Fermi-Dirac distribution (Eq. 2), E_i is related to E_o (Eq. 16) by $E_i \approx E_o + 2k_BT$. Therefore, the points $[E_i, f_0(\Delta E, q)]$ (blue dots in Fig. 7c) approximate the corresponding theoretical points $[E_{opt}, f_0(\Delta E, q)]$ (orange dots in Fig. 7c). The magnitude function $f_m(E_t)$ can be obtained by proper interpolation and extrapolation of experimental data sets $[E_i, f_0(\Delta E, q)]$ with desired E_t resolution and range. According to the simulation, E_i approaches E_{opt} with relative uncertainty < 5% before $f_0(\Delta E, q)$ reaches $0.9 \times \max\{f_m(E_t)\}$. When $f_0(\Delta E, q) > 0.9 \times \max\{f_m(E_t)\}$, replacing "0.87" in Eq. 18 to 0.98 will yield better results.

The other implication is that $f_m(E_t)$ is the envelope of electron population functions derived from a uniform trap depth distribution distribution ($N(E_t) = 1$). From Fig. 7c, for a given charging temperature T_{ch}, the filling function $f(E_t, \Delta E, q, t_c)$ is tangent to the magnitude function $f_m(E_t)$ in a small trap depth range which is illustrated gray in the figure. This means that the envelope constructed from all electron population functions, as done in section III A, is the product of the envelope of filling function, which is $f_m(E_t)$, and an existing trap depth distribution $N(E_t)$. This triggers the method of extracting $N(E_t)$ in the coming paragraphs.

Methods of extracting $N(E_t)$. There are two methods to reconstruct the trap depth distribution $N(E_t)$. The first method relies on the magnitude function $f_m(E_t)$ and the envelope function $n_{env}(E_t, q, t_c)$. The trap depth distribution can be obtained according to,

$$N(E_t) = \frac{n_{env}(E_t, q, t_c)}{f_m(E_t)}. \tag{19}$$

The second method originates from the idea of extracting $N(E_t)$ for the cases with $\Delta E = 0.0$ eV aforementioned. At first, every electron population function $n(E_t, \Delta E, q, t_c)$ is normalized by its magnitude function $f_0(\Delta E, q)$. In this way, every electron population function has the same magnitude of filling, meaning that the influence of ΔE has been removed. In the trap depth range $[E_o(\Delta E, q_1), E_o(\Delta E, q)]$, the value of trap depth distribution can be calculated by,

$$\frac{\Delta\tilde{n}_t(q, t_c)}{\delta E} = \frac{1}{\delta E}\int_{E_a}^{E_b}\left[\frac{n(E_t, q_1, t_c)}{f_0(\Delta E, q_1)} - \frac{n(E_t, q, t_c)}{f_0(\Delta E, q)}\right]dE_t \tag{20}$$

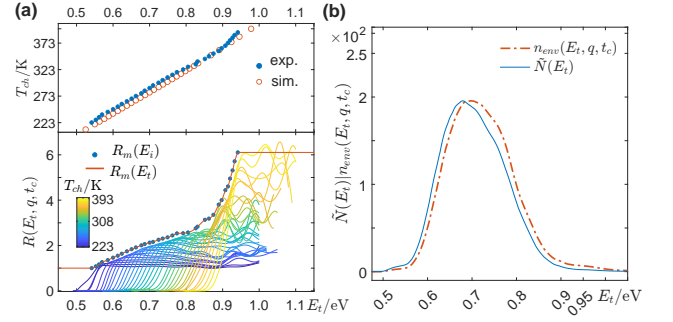FIG. 8. **Approximating the magnitude function**. **(a)** The relative filling function $R(E_t, q, t_c)$ (bottom panel, $q_r \to$ 223 K) approximates the filling function $f(E_t, \Delta E, q, t_c)$. The discrete $[E_i, R_0(\Delta E, q)]$ and the magnitude function $R_m(E_t)$ are displayed as blue dots and an orange line, respectively (bottom panel). The simulated E_i agrees with the experimental ones within a constant difference (top panel). **(b)** The trap depth distribution $\tilde{N}(E_t)$ is calculated from the envelope $n_{env}(E_t, q, t_c)$ by using Eq. 19. Note $n_{env}(E_t, q, t_c)$ has been scaled to share the same magnitude of $\tilde{N}(E_t)$.

in which $\delta E = E_o(\Delta E, q) - E_o(\Delta E, q_1)$, with $q \to T_{ch}$ and $q_1 \to T_{ch} - \Delta T_{ch}$. The trap depth distribution $N(E_t)$ can be approximated by repeating the calculation for electron population functions.

C. Extraction from experiment

As discussed in section III B 2, the first step towards reconstructing $N(E_t)$ is to calculate the filling function $f(E_t, \Delta E, q, t_c)$. This function can be approximated by the following function in a relative manner,

$$R(E_t, q, t_c) = \frac{n(E_t, q, t_c)}{n(E_t, q_r, t_c)}, \tag{21}$$

in which the reference charging condition is $q_r \to T_{ch0}$. $R(E_t, q, t_c)$ is thus termed the relative filling function. For each $R(E_t, q, t_c)$, the magnitude $R_0(\Delta E, q)$ and the corresponding characteristic trap depths E_o and E_i can be extracted. The magnitude $R_0(\Delta E, q)$ is taken as the averaged $R(E_t, q, t_c)$ in a range where it has reached a plateau. Oscillations in $R(E_t, q, t_c)$ bring uncertainties in the extraction. Therefore, an intermediate electron population function $n(E_t, q'_r, t_c)$ is often use to calculate $R(E_t, q, t_c)$, meaning that,

$$R(E_t, q, t_c) = \frac{n(E_t, q, t_c)}{n(E_t, q'_r, t_c)} \times R_0(\Delta E, q'_r). \tag{22}$$

Herein, the charging temperature T'_{ch}(short for $q'_r \to T'_{ch}$) can be chosen to be δT smaller than T_{ch}. The value of δT at one hand should be small enough to reduce oscillations as much as possible since $n(E_t, q, t_c)$ tend to suffer similar uncertainties to that of $n(E_t, q'_r, t_c)$. On the other hand, δT should be large enough to avoid distorting significantly the shape of the $R(E_t, q, t_c)$ in the

E_t range where $R(E_t, q, t_c)$ has not reached the plateau of $R_0(\Delta E, q)$.

After determining the magnitude $R_0(\Delta E, q)$, the characteristic trap depth E_i and E_o can be extracted accordingly. The characteristic trap depth E_i can thus be calculated according to Eq. 18. The relative functions are shown in Fig. 8a (bottom panel). After calculating E_i and $R_0(\Delta E, q)$ for each relative filling function, an approximation to the magnitude function can be constructed,

$$R_m(E_i) : E_i(q) \mapsto R_0(\Delta E, q)$$

which is a discrete analog to Eq. 17 (blue dots in the bottom panel of Fig. 8a). $R_m(E_i)$ can be interpolated for $E_t \in [\min(E_i), \max(E_i)]$, and extrapolated beyond these limits by using $R_m(\min(E_i))$ and $R_m(\max(E_i))$ (Fig. 8a). This leads to the approximated magnitude function $R_m(E_t)$ (orange line in Fig. 8a), i.e.,

$$R_m(E_t) : E_t(q) \mapsto R_0(\Delta E, q), \tag{23}$$

in which E_t is now in the full trap depth range of consideration, i.e. $E_t \in [E_a, E_b]$. As shown in the top panel of Fig. 8a, the experimental E_i is almost linear with the charging temperature T_{ch}. The simulated E_i differs from the experimental one by almost a constant amount for all $q \rightarrow T_{ch}$. The reason of the discrepancy will be discussed in the DISCUSSION section.

Extracting $N(E_t)$ via Eq. 19. Since relative filling functions are used, the approximated trap depth $\tilde{N}(E_t)$ can be calculated by,

$$\tilde{N}(E_t) = \frac{n_{env}(E_t, q, t_c)}{R_m(E_t)}, \tag{24}$$

and the result is shown as blue line in Fig. 8b. The shape of $\tilde{N}(E_t)$ differs slightly from the envelope $n_{env}(E_t, q, t_c)$. The resolution of trap depth of this method is very high, and $R_m(E_t)$ only introduces relatively large uncertainties for $E_t > \max(E_i)$ and $E_t < \min(E_i)$ due to the extrapolation. However, the absolute uncertainties may be smaller because $N(E_t)$ has negligible value in these region. This can be further avoided by extending the range of charging temperatures.

Extracting $N(E_t)$ via Eq. 20. This method is easy to implement as it only requires discrete pairs of $E_o(q)$ and $R_0(\Delta E, q)$. For a pair of charging condition $q \rightarrow T_{ch}$ and $q_1 \rightarrow T_{ch} + \Delta T_{ch}$, the total number of trapped electrons in the range $[E_o(\Delta E, q_1), E_o(\Delta E, q)]$ can be calculated by Eq. 20 upon replacing $f_0(\Delta E, q)$ by $R_0(\Delta E, q)$. The gray area under the normalized electron population functions $n(E_t, q_1, t_c)/R_0(\Delta E, q_1)$ and $n(E_t, q, t_c)/R_0(\Delta E, q)$ in Fig. 9a (bottom panel) actually represents $\Delta \tilde{n}_t(q, t_c)$. The approximated trap depth distribution $\tilde{N}(E_t)$ is shown as a histogram in Fig. 9b, in which $\Delta \tilde{n}_t(q, t_c)$ has been added for illustration purposes. According to Eq. 20, a large uncertainty in $n(E_t, q_1, t_c)/R_0(\Delta E, q_1)$ will lead to large uncertainties
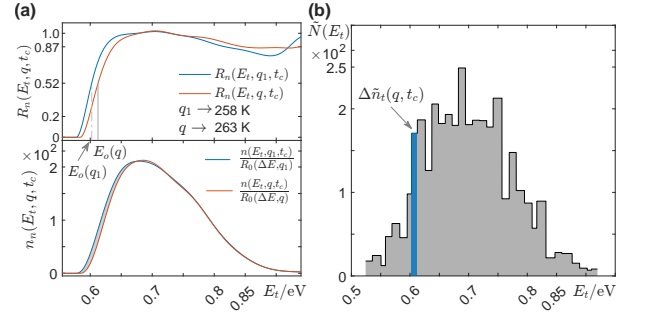

FIG. 9. **Extract $N(E_t)$ via Eq. 20**. (a) The area between two normalized electron population function for q and q_1 characterizes $\Delta \tilde{n}_t(q, t_c)$ (gray area, bottom panel). Here, $R_n(E_t, q, t_c) = R(E_t, q, t_c)/R_0(\Delta E, q)$. (b) The trap depth distribution $\tilde{N}(E_t)$ according to Eq. 20 is represented by a histogram, together with $\Delta \tilde{n}_t(q, t_c)$ for $q \rightarrow 263$ K as a blue bar.
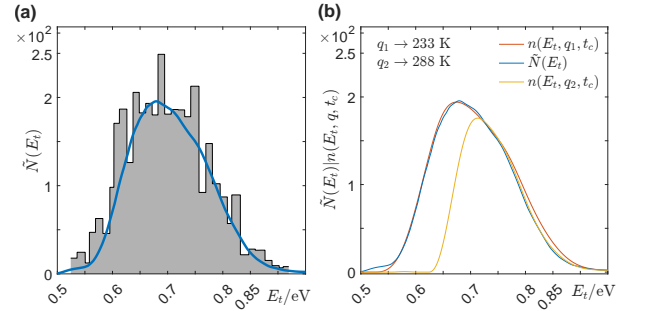

FIG. 10. **Trap depth distribution of $BaSi_2O_2N_2$:2%Eu^{2+}**. (a) The trap distribution $\tilde{N}(E_t)$ extracted by Eq. 24 (blue) agree with that extracted from Eq. 20 (histogram). (b) The electron population function at low charging temperature, e.g. $q_1 \rightarrow 233$ K, can approximate the trap depth distribution $N(E_t)$ but may fail in some ranges.

for two $\Delta \tilde{n}_t(q, t_c)$. This explains the occurrence of several pairs of "high +low" bin heights in the histogram (Fig. 9).

The two methods above reach a consistent trap depth distribution $\tilde{N}(E_t)$ (Fig. 10a). This validates the methods based on simulations in section III B 2. The method of Eq. 24 yields improved precision and resolution of E_t. It is noteworthy that an electron population function at low charging temperature, e.g. $q \rightarrow 233$ K, can approximate the shape of $\tilde{N}(E_t)$ to a satisfactory extent (see $n(E_t, q, t_c)$ in Fig. 10b). For higher charging temperature, only a part of the underlying trap depth can be revealed by the electron population function , e.g. $n(E_t, q_2, t_c)$ in Fig. 10b (yellow line). The discrepancy between $\tilde{N}(E_t)$ and $n(E_t, q, t_c)(q \rightarrow 223$ K) reveals possible error sources from the electron population function or the procedure of extracting trap depth distributions. Therefore, the trap depth distributions can be evaluated to the first-order approximation by the electron population function $n(E_t, q, t_c)$ with the lowest possible charg-
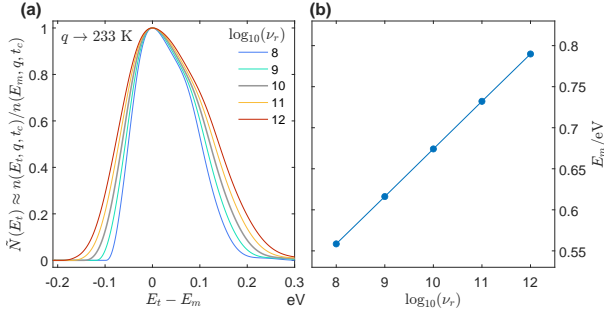
FIG. 11. **The influence of the recombination frequency factor ν_r. (a)** Changing the frequency ν_r to $a\nu_r$ by multiplying a positive scalar a will compress ($a < 1$) or stretch ($a > 1$) the trap depth distribution and then shift it along the E_t axis. **(b)** The value of trap depth E_m increases almost linearly with increasing $\log_{10}(\nu_r)$. Note the trap depth distribution can be approximated by the normalized electron population function $n(E_t, q, t_c)/n(E_m, q, t_c)(q \to 233$ K), with $n(E_m, q, t_c)$ and E_m being the maximum of $n(E_t, q, t_c)$ and the corresponding trap depth, respectively.

ing temperature, as long as the signal strength of the TL curve is still strong enough for the Tikhonov regularization process. This is beneficial for fast screening of persistent phosphors based on their trap depth distributions.

The influence of the frequency factor ν_r. The current model assume a fixed frequency factor of $\nu_r = 10^{10}$ Hz. Scaling ν_r by a positive scalar a will compress ($a < 1$) or stretch ($a > 1$) the trap depth distribution and then shift it along the E_t axis. As revealed in previous sections, the trap depth distribution can be approximated by an normalized electron population function, i.e., $\tilde{N}(E_t) \approx n(E_t, q, t_c)/n(E_m, q, t_c)(q \to 233$ K). Here, $n(E_m, q, t_c)$ and E_m are the maximum of $n(E_t, q, t_c)$ and the corresponding trap depth, respectively. As shown in Fig. 11a, the shape of the trap depth distribution is compressed or stretched for frequency factor ν_r less than or greater than 10^{10} Hz, respectively. The value of E_m gives an estimation of the overall position of the trap depth distribution along the E_t axis. It is obvious that E_m scales almost nearly with $\ln(\nu_r)$ (Fig. 11b). This means the influence of scaling the frequency factor is on an logarithmic order. Hence, small deviation from the chosen frequency factor hardly impose significant impact on the trap depth distribution.

IV. DISCUSSION

A. Interpretation of the model

Approximating the kernel. The temperature integral Eq. 5 decreases almost exponentially with decreasing temperature T. The influence of $F(E_t, T_0)$ on the kernel $K(E_t, T)$ Eq. 4b is mainly located at low temperature (high values in the contour plot in Fig. 3). The

term $F(E_t, T_0)$ is thus sufficiently smaller than $F(E_t, T)$ and can be neglected in Eq. 4b when T is about 20∼30 K greater than T_0 for traps with sufficiently large trap depth. The kernel $K(E_t, T)$ Eq. 4b now reads as,

$$K(E_t, T) = \frac{W(e\nu_r T/\beta)}{T}\exp\left[-\frac{E_t - E_s(T)}{k_\mathrm{B}T}\right.$$
$$\left. - \exp\left(-\frac{E_t - E_s(T)}{k_\mathrm{B}T}\right)\frac{(E_s(T) + k_\mathrm{B}T)/E_t}{\sqrt{1 + 4k_\mathrm{B}T/E_t}}\right],$$
(25a)

$$E_s(T) = k_\mathrm{B}T\left[W(e\nu_r T/\beta) - 1\right],$$
(25b)

where $W(x)$ is the Lambert function of the 0th branch. (The derivation is given in section VI of SM [46].) When $E_s(T)$ is several $k_\mathrm{B}T$ smaller than E_t, the kernel Eq. 25 can be further simplified as,

$$K(E_t, T) \approx \frac{\nu_r}{\beta}\exp\left(-\frac{E_t}{k_\mathrm{B}T}\right),$$

which lays the foundation for the initial rise method. The implicit assumption means that the extracted trap depth will be underestimated upto several $k_\mathrm{B}T$. The magnitude of the kernel $K(E_t, T)$, which is $W(e\nu_r T/\beta)/T$, decays with increasing temperature T. The shape of $K(E_t, T)$ is close to the probability density function (PDF) of the Gumbel distribution [64], and the standard deviation is proportional to $k_\mathrm{B}T$. This means the kernel is mainly distributed several $k_\mathrm{B}T$ around E_s and a linear band structure can be found in the discrete $K(E_t, T)$ (Fig. 3a). Hence, the information of electron population function gets more smeared out in TL curves when temperature increases, which is one of the reasons to apply Tikhonov regularization method.

At large argument x, the derivative $W'(x) = [x + \exp(W(x))]^{-1}$ is close to zero. Hence, the Lambert function in Eq. 25b can be replaced by its averaged value $\langle W \rangle$ in a reasonable temperature range (e.g. 100 to 600 K), and Eq. 25b becomes

$$E_s(T) \approx \langle W \rangle k_\mathrm{B}T$$
(26)

This clearly indicate a linear relationship between temperature T and the characteristic trap depth $E_s(T)$, which has been shown in Fig. 3a. For a delta distribution $N_0\delta(E_t - E_0)$, the trap depth E_0 can be estimated from the temperature of TL maxima, i.e. T_m, via Eq. 25b. For a fixed $\nu_r/\beta = 10^9$, the Urbach relation is recovered, i.e. $E_s(T_m) \approx 23.3k_\mathrm{B}T_m \approx T_m/500$ [24].

A special case of TL is the isothermal thermoluminescence, known as persistent luminescence (PersL). After charging the phosphor at T_{ch}, the temperature of the phosphor still remains unchanged while the luminescence intensity is recorded as a function of delay time t_0, i.e. $I(t_0)$, which is often called the decay profile for the PersL. The PersL intensity $I(t_0)$ can be also written in the in the integral equation,

$$I(t_0) = \int_0^\infty n(E_t, q, t = 0)K(E_t, t_0)dE_t,$$
(27)

with kernel,

$$K(E_t, t_0) = \frac{1}{t_0}\exp\left[-\frac{E_t - E_s(t_0)}{k_{\mathrm{B}}T_{ch}}\right.$$
$$\left. - \exp\left(-\frac{E_t - E_s(t_0)}{k_{\mathrm{B}}T_{ch}}\right)\right] \quad (28a)$$

$$E_s(t_0) = k_{\mathrm{B}}T_{ch}\ln(\nu_r t_0), \quad (28b)$$

which follows the PDF of the Gumbel distribution [64]. This immediately indicates the presence of the power law of $t_0^{-\alpha}$ ($\alpha \approx 1$) for the decay profile, which has been observed in many persistent phosphors [65, 66]. In theory, trap parameters can also be inferred from the PersL decay profile $I(t_0)$ [48, 67]. The shape of the kernel $K(E_t, t_0)$ remains unchanged, but its magnitude t_0^{-1} will scale down the light output from deep traps significantly. This requires both huge delay time t_0 to probe a wide trap trap range and highly sensitive detectors with high dynamic range to register $I(t_0)$ out of noises. However, the decay profile $I(t_0)$ can be used in conjunction with TL curves to understand materials properties to a deeper extent [28, 68].

Frequency factor ν_r. The frequency factor ν_r has been fixed to 10^{10} Hz for regularization in this paper. There are methods to extract the frequency factor, for example see Ref. [50, 69], but they are obtained by assuming there exists only one trap depth. Recently, McKeever and Sholom proposed a sophisticated method of extracting both distributed trap depth and frequency factor [70]. The precise determination asks for detailed knowledge of TL and PersL, and carefully designed experiments. Here, we consider the effect of scaling ν_r by a positive scalar a on the obtained trap depth distribution, which has been illustrated in section III C.

The Lambert function can be expanded as,

$$W(x) \approx \ln(x) - \ln\left[\ln(x)\right],$$

at large argument x [71]. Hence, the characteristic trap depth can be approximated as,

$$E_s(T, a\nu_r) \approx \left[\langle W \rangle + \ln(a)\right] k_{\mathrm{B}}T.$$

This shows that the extracted electron population function can be scaled in the E_t axis due to the term $\ln(a)$. Furthermore, the position of the electron population function, which was estimated by E_m (section III C), will be shifted along the E_t by an amount that is proportional to $\ln(a)$. The extracted trap depth distribution can be altered in similar manners since it can be approximated by an electron population function for low-enough charging temperature (e.g. $n(E_t, q, t_c)$ with $q \to 233$ K).

The optimally charged trap depth. The linear relationship between the charging temperature and the associated trap depth which can be optimally charged (see Fig. 7), can be understood to a satisfactory extent. We set σ_{osl} to zero without loosing generality. At a given

charging condition q, the magnitude of filling,

$$f_0(\Delta E, q) = \frac{k_{\mathrm{trap}}(\Delta E, q)}{k_{\mathrm{trap}}(\Delta E, q) + k_{\mathrm{rcb}}(E_t, q)}$$
$$= \left[1 + \frac{\nu_r k_{\mathrm{rad}}}{\nu_t \sigma_{\mathrm{abs}} I_e(\lambda)}\exp\left(-\frac{E_t - \Delta E}{k_{\mathrm{B}}T}\right)\right]^{-1}, \quad (29)$$

increases with increasing E_t ($\sigma_{\mathrm{osl}} = 0$). Meanwhile, the remainder of Eq. 13,

$$1 - \exp\left[-\left(k_{\mathrm{trap}}(\Delta E, q) + k_{\mathrm{rcb}}(E_t, q)\right)t_{ch}\right],$$

decreases with increasing E_t. This leads to a trap depth at which the phosphor can be charged to the largest efficiency at the given charging temperature T_{ch} (Fig. 7a, bottom panel). This sets the relationship between T_{ch} and E_{opt}. It is interesting to note that the magnitude $f_0(\Delta E, q)$ shows an effective activation energy of $E_t - \Delta E$ to 100% filling.

First-order kinetics. We now turn to the first-order kinetics, which determines the validity of the methods. The first-order kinetics originate from the isolated pairs assumption, without considering retrapping pairs (section III B 1). First order kinetics are assumed for both detrapping during TL and the filling of traps during charging. The retrapping process is the origin of the non-first-order kinetics. Yet, the experimental conditions can be carefully designed to minimize the effect of retrapping. According to the charging procedure (see section II), the phosphor was charged at large irradiance and long charging duration to reach saturated electron population function. In this way, non-first order kinetics during charging can be smeared out into the thermal equilibrium. The cooling process (to T_0) after charging further reduces the non-first-order kinetics. At a given temperature T during the heating process of a TL experiment, the electron at a trap with trap depth E_t can be retrapped into other traps with trap depth i) smaller than or ii) equal to or iii) grater than E_t. In case i) and ii), retrapped electrons will be detrapped at a rate no less than that of the electron at traps with E_t. When electrons are retrapped into deeper traps, they are delayed to be released, increasing the signal strength of TL at higher temperature side. This effect can not be discerned from first-order detrapping from a trap depth depth distribution that show slightly larger values for deep traps.

The effect of retrapping can be observed when the density of electrons at the excited states is increased significantly to enhance the trapping rate. Many experimental observations have been reported. For example, optically stimulated detrapping transfer electrons from deep traps into shallower traps [72, 73]. Even dynamical pressure can transfer electrons from traps of intermediate trap depth into deeper traps [38].

According to the local model, the isolated pairs are assumed. The density of electrons at the excited state of traps are small enough to suppress the observation of the

retrapping process. Hence, the limited rate of retrapping process is not likely to pose a large impact on the methods of extracting the trap depth distribution.

B. Analysis of uncertainties

The accuracy of the extracted trap depth distribution relies on the theoretical framework that suggests the methods of extracting information. The most important implication of the first-order kinetics of charging is the presence and scientific significance of the magnitude function $f_m(E_t)$ Eq. 17 (or the relative version $R_m(E_t)$, Eq. 23). At one hand, $f_m(E_t)$ is the magnitude that should be used to correct electron population functions for variable charging temperature to remove the influence of the thermal barrier ΔE. This directly results in the method via Eq. 20. On the other hand, $f_m(E_t)$ is also the envelope of the electron population functions at variable T_{ch} originating from a uniform trap depth distribution $N(E_t) = 1$. Evidently, the trap depth distribution can be recovered by using the envelope $n_{env}(E_t, q, t_c)$ and the magnitude function $f_m(E_t)$ according to Eq. 19. These deductive methods do not depend on the parameters used in the simulation but depend on the presence of the thermal barrier ΔE. The influences of ΔE can be canceled out via Eq. 19 or Eq. 20 without knowing the exact value of ΔE. Systematic errors are thus minimized, and random errors originate from how to calculate the electron population functions and the associated magnitude function directly.

Consistent setting for charging should be guaranteed to an extent as much as possible. It is advised to cool the phosphor after charging to T_0 at a fast cooling rate such that the electron population function $n(E_t, q, t_c)$ $(q \to T_0)$ can be best approximated by $n(E_t, q, t = 0)$ $(q \to T_{ch})$. The charging irradiance $I_e(\lambda)$ and charging duration t_{ch} should be large enough to produce high signal strength and also a stable shape of electron population function. A detailed analysis can be found in section V of SM [46]. Noises should be minimized as well in order to increase the signal-to-noise ratio. These are important to generate high-quality electron population functions via Tikhonov regularization, which is sensitive to noises. Hence, the importance of acquiring highly consistent and high-quality data can not be emphasized more.

Numerical uncertainties mainly originate from the relative filling function $R(E_t, q, t_c)$ and the methods to extract the magnitude $R_0(\Delta E, q)$ and the characteristic trap depths E_o (Eq. 15) and E_i (Eq. 18). The regularization method can yield small oscillations in the electron population functions because it uses oscillatory singular vectors to reconstruct solutions. The oscillation in $R(E_t, q, t_c)$ can be reduced by choosing an optimized reference electron population function (Eq. 22), leading to a more reliable magnitude $R_0(\Delta E, q)$. The characteristic trap depth E_i from Eq. 18 will yield a few percent

of uncertainties from theory. Large uncertainties may arise when there is an oscillation of $R(E_t, q, t_c)$ before it reaches the magnitude. This has been shown for those $E_i \in (0.8, 0.9)$ eV in Fig. 8.

The method of extracting trap depth distributions via Eq. 19 suffers from uncertainties originating from both $R_m(E_t)$ and the envelope of electron population function $n_{env}(E_t, q, t_c)$. Meanwhile, the method via Eq. 20 is prone to error in the $n_t(q, t_c)$ and the magnitude $R_0(\Delta E, q)$. As the method of difference is used, a large uncertainty in $n_t(q, t_c)/R_0(\Delta E, q)$ will definitely produce large uncertainties in $N(E_t)$ in two consecutive trap depth ranges. This can be confirmed by several pairs of "high+low" height of bins in the histogram of $\tilde{N}(E_t)$.

C. Application of the method

The present model assumes the presence of only one luminescent center and only one thermal barrier. Real persistent phosphors can have multiple luminescent centers or one kind of luminescent center at multiple crystallographic sites, each providing its own emission spectrum and thermal barrier. In these cases, the first-order kinetics must be applied to each distinctive trapping-recombination process independently and the output is the sum of these independent processes. It is noteworthy that the recording of the TL intensity should be spectrally resolved to distinguish the contribution of recombination processes.

Trap depth distributions have found many ways in technological applications. The obvious one is to understand and tune the PersL behavior of persistent phosphors. For example, the trap depth distribution in garnet phosphors can be tuned by alloying to optimize optical storage properties [74]. Furthermore, it provides an estimate for the optimum charging and working temperature (T_{opt}) of persistent phosphors. The quantity $I(t_0)t_0$ can be used to quantify the luminescence decay profile. It combines the effect of intensity of afterglow and the noise level. According to Eq. 28, the kernel $K(E_t, t_0)$ can be approximated by a boxcar function $\text{rect}\left(\frac{E_t - E_o(t_0)}{\pi k_B T_{ch}/\sqrt{6}}\right)$, leading to,

$$I(t_0)t_0 \approx \frac{\pi}{\sqrt{6}} k_B T_{ch} \times n(E_s(t_0), q, t = 0) \qquad (30)$$

which clearly indicates the influence of charging temperature and the trap depth distribution. The charging temperature T_{ch} that maximizes $I(t_0)t_0$ can be estimated by examining the maximum of $N(E_t)$. For the model phosphor $BaSi_2O_2N_2$:2%Eu^{2+}, this optimum charging temperature is around 288 K, which results in an electron population function with its maximum located around that of the trap depth distribution (yellow line, Fig. 10b). This prediction can be compared with further experimental verification.

Given the trap depth distribution $\tilde{N}(E_t)$, it is also easy to simulate the decay profile for PersL or the TL pro-

files at different charging and working conditions. This helps to explain and predict the properties of phosphors. More importantly, the trap distribution can be used as a reliable feature of persistent/storage phosphors. This facilitates the discovery of empirical laws that govern the properties of persistent phosphors via machine learning.

V. CONCLUSION

In this contribution, a method was proposed to extract the trap distribution from thermoluminescene (TL) curves with the presence of a thermal barrier for charging. It is based on a local transition model that leads to first-order kinetics of charge transitions. The model predicts the evolution of the filling function as a function of charging temperature. Firstly, the electron population functions $n(E_t, T_{ch}, t_c)$ and the envelope $n_{env}(E_t, q, t_c)$ were obtained from the corresponding TL curves by the Tikhonov regularization method. Secondly, the relative magnitude of the filling function, i.e., $f_m(E_t)$, is estimated out of ratios of electron population functions. Finally, the trap depth distribution can be estimated according to either $N(E_t) = n_{env}(E_t, q, t_c)/f_m(E_t)$ (Eq.

19) or Eq. 20. The methods do not require the value of the thermal barrier ΔE beforehand, although ΔE influences the filling functions. Our case study on $BaSi_2O_2N_2$:Eu^{2+} validated this method. A broad trap depth distribution, ranging from 0.5 to 0.9 eV with the maximum around 0.65 eV, was revealed, assuming a frequency factor of $\nu_r = 10^{10}$ Hz.

The method via Eq. 19 not only shows a clear physics picture but also yields high precision and resolution of trap depth, provided that TL curves with high signal strength and high signal-to-noise ratio are available. The trap distribution definitely promotes the understanding and tailoring of the properties of persistent phosphors and storage phosphors.

ACKNOWLEDGMENTS

[1] K. Van den Eeckhout, P. F. Smet, and D. Poelman, Persistent luminescence in Eu^{2+}-doped compounds: A review, Materials **3**, 2536 (2010).

[2] K. Van den Eeckhout, D. Poelman, and P. F. Smet, Persistent luminescence in non-Eu^{2+}-doped compounds: A review, Materials **6**, 2789 (2013).

[3] J. Xu and S. Tanabe, Persistent luminescence instead of phosphorescence: History, mechanism, and perspective, J. Lumin. **205**, 581 (2019).

[4] D. Poelman, D. Van der Heggen, J. Du, E. Cosaert, and P. F. Smet, Persistent phosphors for the future: Fit for the right application, J. Appl. Phys. **128**, 240903 (2020).

[5] P. F. Smet, K. Van den Eeckhout, O. Q. De Clercq, and D. Poelman, Chapter 274 - persistent phosphors, in *Including Actinides*, Handbook on the Physics and Chemistry of Rare Earths, Vol. 48, edited by J.-C. Bünzli and V. K. Pecharsky (Elsevier, 2015) pp. 1–108.

[6] T. Lyu and P. Dorenbos, Towards information storage by designing both electron and hole detrapping processes in bismuth and lanthanide-doped $LiRE(Si,Ge)O_4$ (RE = Y, Lu) with high charge carrier storage capacity, Chem. Eng. J. **400**, 124776 (2020).

[7] J. Du, O. De Clercq, and D. Poelman, Temperature dependent persistent luminescence: Evaluating the optimum working temperature, Sci. Rep. **9**, 10517 (2019).

[8] J. Du, A. Feng, and D. Poelman, Temperature dependency of trap-controlled persistent luminescence, Laser Photonics Rev. **14**, 2000060 (2020).

[9] A. Y.-T. Wang, R. J. Murdock, S. K. Kauwe, A. O. Oliynyk, A. Gurlo, J. Brgoch, K. A. Persson, and T. D. Sparks, Machine learning for materials scientists: An introductory guide toward best practices, Chem. Mater.

32, 4954 (2020).

[10] J. Botterman, J. J. Joos, and P. F. Smet, Trapping and detrapping in $SrAl_2O_4$:Eu, Dy persistent phosphors: Influence of excitation wavelength and temperature, Phys. Rev. B **90**, 085147 (2014).

[11] C. Tydtgat, K. W. Meert, D. Poelman, and P. F. Smet, Optically stimulated detrapping during charging of persistent phosphors, Opt. Mater. Express **6**, 844 (2016).

[12] P. F. Smet, K. Van den Eeckhout, A. J. Bos, E. v. der Kolk, and P. Dorenbos, Temperature and wavelength dependent trap filling in $M_2Si_5N_8$:Eu (M=Ca,Sr,Ba) persistent phosphors, J. Lumin. **132**, 682 (2012).

[13] J. Ueda, P. Dorenbos, A. J. J. Bos, A. Meijerink, and S. Tanabe, Insight into the thermal quenching mechanism for $Y_3Al_5O_{12}$:Ce^{3+} through thermoluminescence excitation spectroscopy, J. Phys. Chem. C **119**, 25003 (2015).

[14] J. Ueda, A. Meijerink, P. Dorenbos, A. J. J. Bos, and S. Tanabe, Thermal ionization and thermally activated crossover quenching processes for $5d-4f$ luminescence in $Y_3Al_{5-x}Ga_xO_{12}$:Pr^{3+}, Phys. Rev. B **95**, 014303 (2017).

[15] J. Ueda, S. Tanabe, and T. Nakanishi, Analysis of Ce^{3+} luminescence quenching in solid solutions between $Y_3Al_5O_{12}$ and $Y_3Ga_5O_{12}$ by temperature dependence of photoconductivity measurement, J. Appl. Phys. **110**, 053102 (2011).

[16] T. Lesniewski, S. Mahlik, K. Asami, J. Ueda, M. Grinberg, and S. Tanabe, Comparison of quenching mechanisms in $Gd_3Al_{5-x}Ga_xO_{12}$:Ce^{3+} ($x = 3$ and 5) garnet phosphors by photocurrent excitation spectroscopy, Phys. Chem. Chem. Phys. **20**, 18380 (2018).

[17] J. M. Ogiegło, A. Katelnikovas, A. Zych, T. Jüstel, A. Meijerink, and C. R. Ronda, Luminescence and lu-

minescence quenching in $Gd_3(Ga,Al)_5O_{12}$ scintillators doped with Ce^{3+}, J. Phys. Chem. A **117**, 2479 (2013).

[18] J. Ueda and S. Tanabe, (INVITED) Review of luminescent properties of Ce^{3+}-doped garnet phosphors: New insight into the effect of crystal and electronic structure, Opt. Mater.: X **1**, 100018 (2019).

[19] D. Van der Heggen, J. Joos, D. Rodríguez Burbano, J. Capobianco, and P. F. Smet, Counting the photons: Determining the absolute storage capacity of persistent phosphors, Materials **10**, 867 (2017).

[20] R. Chen, On the calculation of activation energies and frequency factors from glow curves, J. Appl. Phys. **40**, 570–585 (1969).

[21] P. Kivits and H. Hagebeuk, Evaluation of the model for thermally stimulated luminescence and conductivity; reliability of trap depth determinations, J. Lumin. **15**, 1 (1977).

[22] G. F. J. Garlick and A. F. Gibson, The electron trap mechanism of luminescence in sulphide and silicate phosphors, Proc. Phys. Soc. **60**, 574 (1948).

[23] A. C. Coleman and E. G. Yukihara, On the validity and accuracy of the initial rise method investigated using realistically simulated thermoluminescence curves, Radiat. Meas. **117**, 70 (2018).

[24] F. Urbach, Zur lumineszenz der alkalihalogenide, Sitzungsberichte Akad. der Wiss. Wien **139**, 363 (1930).

[25] H. Gobrecht and D. Hofmann, Spectroscopy of traps by fractional glow technique, J. Phys. Chem. Solids **27**, 509 (1966).

[26] A. Chruścińska, The fractional thermoluminescence: some aspects concerning the experimental data analysis, J. Lumin. **62**, 115 (1994).

[27] S. W. S. McKeever, On the analysis of complex thermoluminescence glow-curves: Resolution into individual peaks, Phys. Status Solidi A **62**, 331 (1980).

[28] V. M. Khanin, I. I. Vrubel, R. G. Polozkov, I. A. Shelykh, I. D. Venevtsev, A. Meijerink, H. Wieczorek, J. Boerekamp, S. Spoor, P. A. Rodnyi, and C. Ronda, Modeling and assessment of afterglow decay curves from thermally stimulated luminescence of complex Garnets, J. Phys. Chem. A **123**, 1894 (2019).

[29] P. Bräunlich, ed., *Thermally stimulated relaxation in solids*, Topics in applied physics No. 37 (Springer, Berlin, Heidelberg, 1979).

[30] D. Van der Heggen, J. J. Joos, and P. F. Smet, Importance of evaluating the intensity dependency of the quantum efficiency: Impact on leds and persistent phosphors, ACS Photonics **5**, 4529 (2018).

[31] K. Van den Eeckhout, A. J. J. Bos, D. Poelman, and P. F. Smet, Revealing trap depth distributions in persistent phosphors, Phys. Rev. B **87**, 045126 (2013).

[32] D. Curie, *Luminescence in Crystals*, 1st ed. (Dunod, Paris, 1960).

[33] P. Dorenbos, Thermal quenching of Eu^{2+} 5d-4f luminescence in inorganic compounds, J. Phys.: Condens. Matter **17**, 8103 (2005).

[34] E. Mihóková and M. Nikl, Luminescent materials: Probing the excited state of emission centers by spectroscopic methods, Meas. Sci. Technol. **26**, 012001 (2014).

[35] J. Botterman, K. Van den Eeckhout, A. J. J. Bos, P. Dorenbos, and P. F. Smet, Persistent luminescence in $MSi_2O_2N_2$:Eu phosphors, Opt. Mater. Express **2**, 341 (2012).

[36] A. Feng and P. F. Smet, A review of mechanolumines-cence in inorganic solids: Compounds, mechanisms, models and applications, Materials **11**, 484 (2018).

[37] J. Botterman, K. Van den Eeckhout, I. De Baere, D. Poelman, and P. F. Smet, Mechanoluminescence in $BaSi_2O_2N_2$:Eu, Acta Mater. **60**, 5494 (2012).

[38] R. R. Petit, S. E. Michels, A. Feng, and P. F. Smet, Adding memory to pressure-sensitive phosphors, Light Sci. Appl. **8**, 124 (2019).

[39] V. Bachmann, C. Ronda, O. Oeckler, W. Schnick, and A. Meijerink, Color point tuning for $(Sr,Ca,Ba)Si_2O_2N_2$:Eu^{2+} for white light leds, Chem. Mater. **21**, 316 (2009).

[40] F. Clabau, X. Rocquefelte, T. Le Mercier, P. Deniard, S. Jobic, and M.-H. Whangbo, Formulation of phosphorescence mechanisms in inorganic solids based on a new model of defect conglomeration, Chem. Mater. **18**, 3212 (2006).

[41] G. A. Mandl, D. Van der Heggen, D. R. Cooper, J. J. Joos, J. Seuntjens, P. F. Smet, and J. A. Capobianco, On a local (de-)trapping model for highly doped Pr^{3+} radioluminescent and persistent luminescent nanoparticles, Nanoscale **12**, 20759 (2020).

[42] J. J. Joos, I. Neefjes, L. Seijo, and Z. Barandiarán, Charge transfer from Eu^{2+} to trivalent lanthanide codopants: Systematic behavior across the series, J. Chem. Phys. **154**, 064704 (2021).

[43] B.-G. Yun, T. Horikawa, H. Hanzawa, and K.-i. Machida, Preparation and luminescence properties of single-phase $BaSi_2O_2N_2$:Eu^{2+}, a bluish-green phosphor for white light-emitting diodes, J. Electrochem. Soc. **157**, J364 (2010).

[44] X.-Y. Sun, Z.-P. Ye, Y.-T. Wu, P. Gao, R.-H. Mao, Z.-J. Zhang, and J.-T. Zhao, A simple and highly efficient method for synthesis of Ce^{3+}-activated borogermanate scintillating glasses in air, J. Am. Ceram. Soc. **97**, 3388 (2014).

[45] A. Feng, S. Michels, A. Lamberti, W. Van Paepegem, and P. F. Smet, Relating structural phase transitions to mechanoluminescence: The case of the $Ca_{1-x}Sr_xAl_2Si_2O_8$:1%Eu^{2+},1%Pr^{3+} anorthite, Acta Mater. **183**, 493 (2020).

[46] See supplemental material at `http://link.aps.org/supplemental/10.1103/PhysRevB` for additional information. It includes thermal quenching data, the implementation of regularization method in MATLAB, the method of extracting the envelope, derivation of trapping and recombination coefficients, does dependency of the electron population function, and the derivation of simplified kernels. It includes Refs [45, 56–59, 71, 75–79].

[47] F. I., Sur une Classe d'Equations Fonctionnelles, Acta Math. **27**, 365 (1903).

[48] R. Chen and S. W. S. McKeever, *Theory of Thermoluminescence and Related Phenomena* (World Scientific, Singapore, 1997).

[49] J. H. Flynn, The "temperature integral" - Its use and abuse, Thermochim. Acta **300**, 83 (1997).

[50] J. T. Randall, M. H. F. Wilkins, and M. L. E. Oliphant, Phosphorescence and electron traps I. The study of trap distributions, Proc. R. Soc. Lond. A **184**, 365 (1945).

[51] J. T. Randall and M. H. F. Wilkins, Phosphorescence and electron traps II. The interpretation of long-period phosphorescence, Proc. R. Soc. Lond. A **184**, 390 (1945).

[52] M. Balarin, Improved approximations of the exponential integral in tempering kinetics, J. Therm. Anal. **12**, 169

[53] J. J. M. Órfão, Review and evaluation of the approximations to the temperature integral, AIChE J. **53**, 2905 (2007).

[54] P. Hansen, The discrete picard condition for discrete ill-posed problems, BIT Numer. Math. **30**, 658 (1990).

[55] A. N. Tikhonov and V. Y. Arsenin, *Solutions of ill-posed problems*, Scripta series in mathematics (Winston; distributed solely by Halsted Press, Washington: New York, USA, 1977).

[56] P. C. Hansen, *Discrete Inverse Problems* (Society for Industrial and Applied Mathematics, Philadelphia, USA, 2010).

[57] P. C. Hansen and D. P. O'Leary, The use of the l-curve in the regularization of discrete ill-posed problems, SIAM J. Sci. Comput. **14**, 1487 (1993).

[58] P. C. Hansen, Regularization Tools: A Matlab package for analysis and solution of discrete ill-posed problems, Nume. Algor. **6**, 1 (1994).

[59] P. C. Hansen, Regularization Tools version 4.0 for Matlab 7.3, Numer. Algor. **46**, 189 (2007).

[60] J. J. Joos, P. F. Smet, L. Seijo, and Z. Barandiarán, Insights into the complexity of the excited states of Eu-doped luminescent materials, Inorg. Chem. Front. **7**, 871 (2020).

[61] T. Aitasalo, J. Hölsä, H. Jungner, M. Lastusaari, and J. Niittykoski, Thermoluminescence study of persistent luminescence materials: Eu^{2+}- and R^{3+}-doped calcium aluminates, $CaAl_2O_4$:Eu^{2+},R^{3+}, J. Phys. Chem. B **110**, 4589 (2006).

[62] J. J. Joos, K. Korthout, L. Amidani, P. Glatzel, D. Poelman, and P. F. Smet, Identification of Dy^{3+}/Dy^{2+} as electron trap in persistent phosphors, Phys. Rev. Lett. **125**, 033001 (2020).

[63] C. J. Delbecq, Y. Toyozawa, and P. H. Yuster, Tunneling recombination of trapped electrons and holes in kcl:agcl and kcl:tlcl, Phys. Rev. B **9**, 4497 (1974).

[64] S. Coles, *An Introduction to Statistical Modeling of Extreme Values*, Springer Series in Statistics (Springer London, London, 2001).

[65] W. L. Medlin, Decay of phosphorescence from a distribution of trapping levels, Phys. Rev. **123**, 502 (1961).

[66] D. J. Huntley, An explanation of the power-law decay of luminescence, J. Phys.: Condens. Matter **18**, 1359 (2006).

[67] R. Chen and N. Kristianpoller, Investigation of phosphorescence decay using TL-like presentation, Radiat. Prot. Dosim. **17**, 443 (1986).

[68] V. M. Khanin, I. I. Vrubel, R. G. Polozkov, I. D. Venevtsev, P. A. Rodnyi, T. Tukhvatulina, K. Chernenko, W. Drozdowski, M. E. Witkowski, M. Makowski, E. V. Dorogin, N. V. Rudin, C. Ronda, H. Wieczorek, J. Boerekamp, S. Spoor, I. A. Shelykh, and A. Meijerink, Complex garnets: Microscopic parameters characterizing afterglow, J. Phys. Chem. C **123**, 22725 (2019).

[69] V. Khanin, I. Venevtsev, S. Spoor, J. Boerekamp, A.-M. van Dongen, H. Wieczorek, K. Chernenko, D. Buettner, C. Ronda, and P. Rodnyi, A new method for unambiguous determination of trap parameters from afterglow and TSL curves connection: Example on garnets, Opt. Mater. **72**, 161 (2017).

[70] S. McKeever and S. Sholom, Trap level spectroscopy of disordered materials using thermoluminescence: An ap-

plication to aluminosilicate glass, J. Lumin. **234**, 117950 (2021).

[71] R. Iacono and J. P. Boyd, New approximations to the principal real-valued branch of the lambert W-function, Adv. Comput. Math **43**, 1403 (2017).

[72] P. Avouris and T. N. Morgan, A tunneling model for the decay of luminescence in inorganic phosphors: The case of Zn_2SiO_4:Mn, J. Chem. Phys. **74**, 4347 (1981).

[73] Y. Liang, F. Liu, Y. Chen, K. Sun, and Z. Pan, Long persistent luminescence in the ultraviolet in Pb^{2+}-doped $Sr_2MgGe_2O_7$ persistent phosphor, Dalton Trans. **45**, 1322 (2016).

[74] W. Li, Y. Zhuang, P. Zheng, T.-L. Zhou, J. Xu, J. Ueda, S. Tanabe, L. Wang, and R.-J. Xie, Tailoring trap depth and emission wavelength in $Y_3Al_{5-x}Ga_xO_{12}$:Ce^{3+},V^{3+} phosphor-in-glass films for optical information storage, ACS Appl. Mater. Interfaces **10**, 27150 (2018).

[75] N. F. Mott, On the absorption of light by crystals, Proc. R. Soc. London, Ser. A **167**, 384 (1938).

[76] H. Akima, A new method of interpolation and smooth curve fitting based on local procedures, J. ACM **17**, 589–602 (1970).

[77] E. Kotomin and V. Kuzovkov, eds., *Modern Aspects of Diffusion-Controlled Reactions*, Comprehensive Chemical Kinetics, Vol. 34 (Elsevier, 1996) pp. 1 – 52.

[78] J. F. Perez-Benito, Some considerations on the fundamentals of chemical kinetics: Steady state, quasi-equilibrium, and transition state theory, J. Chem. Educ. **94**, 1238 (2017).

[79] W. Gautschi and W. Cahill, Handbook of mathematical functions: with formulas, graphs, and mathematical tables (Dover Publications, Washington, D.C, USA, 1970) Chap. 5. Exponential Integral and Related Functions, pp. 228–237, 9th ed.

Revealing trap depth distributions in persistent phosphors with a thermal barrier for charging

Ang Feng,[1,2] Jonas J. Joos,[1,2] Jiaren Du,[1,2,3] and Philippe F. Smet[1,2,*]

[1]LumiLab, Department of Solid State Sciences, Faculty of Sciences,
Ghent University, Krijgslaan 281-S1, Gent 9000, Belgium
[2]Center for Nano- and Biophotonics (NB-Photonics), Ghent University, Belgium
[3]International Joint Research Center for Photo-responsive Molecules and Materials,
School of Chemical and Material Engineering, Jiangnan University, Wuxi 214122, China
(Dated: November 16, 2021)

This the supplemental materials (SM) for the paper entitled "Revealing trap depth distributions in persistent phosphors with a thermal barrier of charging." It covers supplementary information on experimental methods, extra experimental data, derivation of formulae and MATLAB code that implementing the regularization method.

I. THERMAL QUENCHING PROFILES

The thermal quenching (TQ) behavior of a phosphor should be inferred from kinetics study of the excited state of the involved luminescent centers. However, more accessible approaches are also used in practice. The phosphor is heated from low temperature to high temperature continuously at a fixed rate while being illuminated by excitation light. The integrated intensity of the emission spectra as a function of temperature is the so-called TQ profile. The electron trapping in persistent phosphors can reduce the emission intensity. Therefore, we adopt the method from Ref [45].

The charging protocol (Fig. S1a) characterizes charging at each $T = 213 + 5i$ K ($i = [0 : 1 : 57]$) for 30 s during heating from 213 to 498 K. The emission spectrum for each charging temperature T was obtained by averaging five spectra from the 24-28$^{\text{th}}$ s of the charging, as shown by the grey shade in Fig. S1a. Each of these spectra (Fig. S1b) was integrated 400 nm to 650 to calculate the emission intensity $I_t(T)$. Then, $I_t(T)$ was normalized with respect to $I_t(213$ K), leading to the TQ profile $I_q(T)$ (Fig. S1c).

The TQ profile (Fig. S1c) was fitted to the single-barrier model [75],

$$I_q(T) = \frac{I_0}{1 + A\exp\left(-\frac{E_q}{k_{\text{B}}T}\right)}, \tag{S1}$$

where E_q is the thermal barrier and k_{B} the Boltzmann constant. I_0 and A are fitting parameters. The fitting results give $I_0 = 0.9676$, $A = 289.4$ and the thermal barrier $E_q = 254.1$ meV.
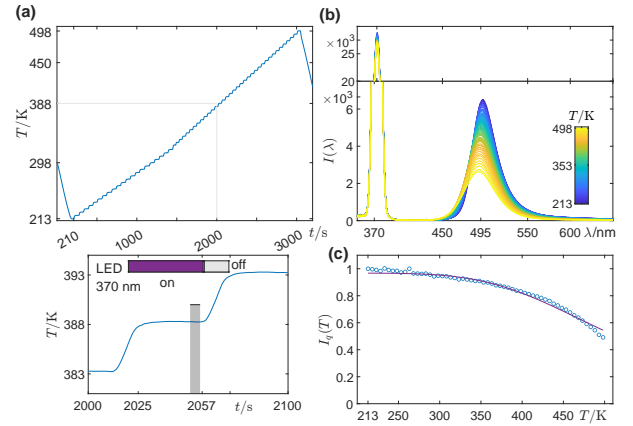

FIG. S1. **Thermal quenching profiles.** (a) The phosphor was warmed up from 213 to 498 K with charging of 30 s at each temperature $T = 213 + 5i$ K ($i = [0 : 1 : 57]$). Five spectra from the 24-28$^{\text{th}}$ s was averaged to $I(\lambda)$ (illustrated in the bottom panel). (b) With increasing T, the intensity of the spectra of excitation light decreases only slightly while that of the emission spectra of BaSi$_2$O$_2$N$_2$:2%Eu^{2+} decreases significantly. (c) The integrated emission intensity (400-650 nm) was normalized to that of $T = 213$ K, and was then fitted to the single barrier model $I_q(T) = I_0/\left[1 + A\exp\left(-\frac{E_q}{k_{\text{B}}T}\right)\right]$. The thermal barrier is found to be $E_q = 0.254$ eV.

II. EXTRACTING ELECTRON POPULATION FUNCTION

In the framework of first-order kinetics, the electron population function $n(E_t, q, t_c)$ is related to the TL intensity $I(t)$ via integral equation Eq. 4 in the paper. The first step to solve these equation is to discretize the integral equation over a grid $[T_0, T_m] \times [E_a, E_b]$. The
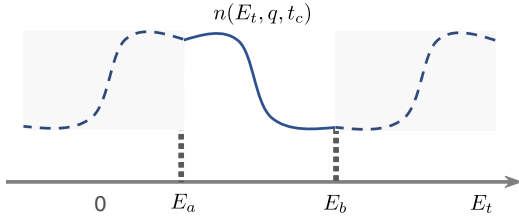
---

* Philippe.Smet@UGent.be

FIG. S2. **Reflexive boundary condition.** The reflexive boundary condition assumes solution $n(E_t, q, t_c)$ outside the interval (E_a, E_b) results from reflecting $n(E_t, q, t_c)$ along $E_t = E_a$ and $E_t = E_b$.

quadrature method with the midpoint rule yields,

$$\sum_{j=1}^{N} \omega_j K\left(E_{tj}, T_k\right) n\left(E_{tj}\right) = I\left(T_k\right), \quad k = 1, 2, ..., M$$
(S2)

or in the matrix form (Eq. 6 in the paper),

$$Kn = I,$$
(S3)

with $K_{kj} = \omega_j K\left(E_{tj}, T_k\right), n_j = n\left(E_{tj}\right), I_k = I\left(T_k\right),$ and $\omega_j = \frac{E_b - E_a}{N}$. Note, here I is obtained by interpolating the cleaned experimental TL data onto the temperature vector `t = T0+(0.5:1:M-0.5)'*dT`, with `dT=(Tm-T0)/M`. It is not possible to solve Eq. S3 via the standard least square method due to the noise of TL signal and a huge condition number of $K(E_t, T)$. The Tikhonov regularization method boils down to solve,

$$\begin{bmatrix} K \\ \lambda L \end{bmatrix} n = \begin{bmatrix} I \\ 0 \end{bmatrix},$$
(S4)

with an optimized regularization parameter λ that minimizes the functional,

$$V(\hat{n}) = \|K\hat{n} - I\|_2^2 + \lambda^2 \|L\hat{n}\|_2^2.$$
(S5)

Herein, L is the discrete approximation of a derivative operator. To solve this problem, we adopt the reflexive boundary condition. It assumes that $n(E_t, q, t_c)$ for $E_t < E_a$ and $E_t > E_b$ results from reflecting $n(E_t, q, t_c)$ along $E_t = E_a$ and $E_t = E_b$, respectively (Fig. S2). Under such a condition, the kernel is now,

$$\begin{aligned} K\left(E_t, T\right)_r =& K\left(E_t, T\right) \\ &+ K\left(2E_a - E_t, T\right) \\ &+ K\left(2E_b - E_t, T\right), \end{aligned}$$
(S6)

subjected to $K\left(2E_a - E_t, T\right) = 0$ when $2E_a - E_t < 0$. Furthermore, the discrete approximation of a second derivative operator L can be written as [56],

$$L = \begin{bmatrix} -1 & 1 & & & \\ 1 & -2 & 1 & & \\ & \cdot & \cdot & \cdot & \\ & & 1 & -2 & 1 \\ & & & 1 & -1 \end{bmatrix}_{N \times N}.$$
(S7)

A generalized singular value decomposition (GSVD) method is utilized to decompose K and L simultaneously so that the solution is given by,

$$n_{L,\lambda} = \sum_{k=1}^{N} \phi_k^{[L,\lambda]} \frac{u_k'^T I}{\sigma_k'} n_k',$$
(S8)

where the ratio σ_k'/μ_k' (with $\sigma_k'^2 + \mu_k'^2 = 1$) is the generalized singular values. The right singular vectors n_k', which are shared by both L and A, are mutually independent but are neither normalized nor orthogonal. There are two sets of left GSVD orthonormal vectors u_k' and v_k' satisfy

$$Kn_k' = \sigma_k' u_k', \quad Ln_k' = \mu_k' v_k'.$$

Here we provide the MATLAB code that solves $n(E_t, q, t_c)$ from TL data by using the *Regularization Tools* MATLAB package [58, 59]. We assume the package has been added to the search path of MATLAB installation.

- Discretization.

```
1   kB = 0.08617; nu = 1e10; beta = 0.5;
2   T0 = 213.15; Tm = 473.15; %T range, K
3   Ea = 300; Eb = 1200; % Et range, meV
4   N = 3200; M = ceil(N/2); % # of
       intervals
5   de = (Eb-Ea)/N; dT = (Tm-T0)/M;
6   e = Ea+(0.5:N-0.5)'*de; t = T0+(0.5:M
       -0.5)'*dT;
7   [E,T] = meshgrid(e,t); % meshgrid on
       the EtxT plane;
8   tInt = @(x,y) kB*nu/beta*(y.^2./x).*...
9   exp(-x./y/kB)./sqrt(1+4*kB*y./x); % x--
       Et, y--T; Ref. M Balarin J therm
       Anal 12, 169 (1977).
10  TempInt = @(x,y) tInt(x,y)-tInt(x,T0);%
       temperature integral
11  Kf = @(x,y) de*nu/beta*exp(-x./(kB*y)-
       TempInt(x,y));
12  K1 = Kf(E,T); K2 = Kf(2*Eb-E,T);
13  K3 = Kf(2*Ea-E,T);
14  zIdx = (2*Ea-E)<0; K3(zIdx) = 0;
15  K = K1+K2+K3;
16  L = diag([-1;ones(N-2,1)*(-2);-1]);
17  L(2:N,1:N-1) = L(2:N,1:N-1) +...
18    diag(ones(N-1,1));
19  L(1:N-1,2:N) = L(1:N-1,2:N) +...
20    diag(ones(N-1,1));
```

- GSVD.

```
1   [U,sm,X,V,W] = cgsvd(K,L).
```

- Denoise TL signal. The temperature and the corresponding TL intensity are stored in the first and second columns of a matrix `TL`, respectively. These quantities can will be first extracted and denoised by wavelet methods.

```
1  TLt = TL(:,1)+273.15; %temperature
2  TLint = TL(:,2); %TL intensity
3  TLint_den = wdenoise(TLint);%wavelet
       denoising.
```

The signal `TLint_den` was further denoised by the stationary wavelet transform (SWT) implemented in the Wavelet Analyzer APP of MATLAB. In this process, the signal will be first extended to the required length and then be denoised by using the `haar` wavelet to 3 levels of denoising. The cleaned signal is saved as `TLintp`. Afterwards, it will then be interpolated to the temperature vector by using the spline method.

```
1  b = interp1(TLt,TLintp,t,'spline'); %
       iterpolation
```

- Choose λ_{opt}. The optimized regularization parameter λ_{opt} can be found from the corner of the L-curve [57], which can be calculated from GSVD of the problem. This involves solving Eq. S4 by a series of sampled parameters via the `l_curve` function,

```
1  [lambda_opt,~,~,~] = l_curve(U,...
2  sm,b,'Tikh',L,V);
```

where the desired parameter λ_{opt} is `lambda_opt`.

- Solve $\mathbf{x}_\lambda$. A non-negativity constraint on $\mathbf{x}_\lambda$ is usually assumed. The constraint-free solution `x_lambda` will be calculated by calling the `tikhonov` function. The solution is bounded at zero and will be treated as the initial solution to a non-negative linear least square problem (Eq. S4), which yields non-negative solution `xhat`.

```
1   [x_lambda,~,~] =  tikhonov(U,sm,...
2   X,b,lambda_opt);
3   bhat = [b;zeros(size(L(:,1)))];
4   xhat0 = x_lambda; xhat0(xhat0<0)=0.0;
5   lowerbound = zeros(size(xhat0));
6   upperbound = ones(size(xhat0)).*...
7   max(xhat0)*1.2;
8   opts.Algorithm = 'trust-region-
        reflective';
9   opts.SubproblemAlgorithm = '
        factorization'; %
10  Ahat = [K;lambda_opt*L];
11  xhat = lsqlin(Ahat,bhat,[],[],[],...
12  [],lowerbound,upperbound,xhat0,opts);
13  %constrained linear least square
```

III. EXTRACTING THE ENVELOPE

The envelope $n_{env}(E_t, q, t_c)$ can be extracted from electron population functions $n(E_t, q, t_c)$ with all chosen
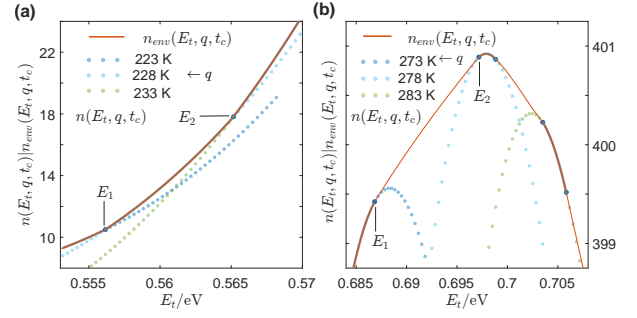

FIG. S3. **Constructing the envelope**. **(a)** In certain E_t ranges, the envelope $n_{env}(E_t, q, t_c)$ can be fully constructed by taking parts of data from $n(E_t, q, t_c)$ with consecutive T_{ch}. **(b)** In some E_t ranges, interpolation is applied to calculate $n_{env}(E_t, q, t_c)$ when data points from $n(E_t, q, t_c)$ do not yield satisfactory results. The grey thick lines outline the intersection of $n_{env}(E_t, q, t_c)$ and $n(E_t, q, t_c)$ with the endpoint shown in deep blue dots.

charging temperature T_{ch}. In some E_t range, the envelope $n_{env}(E_t, q, t_c)$ can be directly taken from the electron population function $n(E_t, q, t_c)$. This is illustrated in Fig. S3a. The electron population function $n(E_t, q, t_c)$ intersect with $n(E_t, q_1, t_c)$ and $n(E_t, q_2, t_c)$ at E_1 and E_2, respectively, where

$$q \to 228 \text{ K}, q_1 \to 223 \text{ K}, q_2 \to 233 \text{ K}.$$

Thus, $n_{env}(E_t, q, t_c) \approx n(E_t, q, t_c)$ in the range (E_1, E_2) and this approximation is highlighted by a grey line. However, this method may lead to unwanted artifacts in certain ranges. For example in Fig. S3b, the electron population function $n(E_t, q, t_c)$ is expected to have its maximum between 339.5 and 401, which is higher than the value extracted by the aforementioned method. Hence, no data points were taken from electron population functions in the range (E_1, E_2). All extracted data points will be interpolated in the full range $E_t \in (E_a, E_b)$ by the method proposed by H. Akima [76]. It is clear that the interpolation provide acceptable results in the range (E_1, E_2) where no data points were taken from $n(E_t, q, t_c)$.

It noteworthy that the envelope should be tangent to electron population functions. Hence, the choice of data points from electron population function, as illustrated in Fig. S3, should meet this requirement. The interpolation method by H. Akima was chosen here because it avoids overshoots [76].

IV. TRAPPING AND RECOMBINATION COEFFICIENTS

A luminescent center (Fig. S4) can be represented by its ground state and the excited state. This is also true for a trap. Within the framework of isolated pair approximation, trapping and recombination only takes place
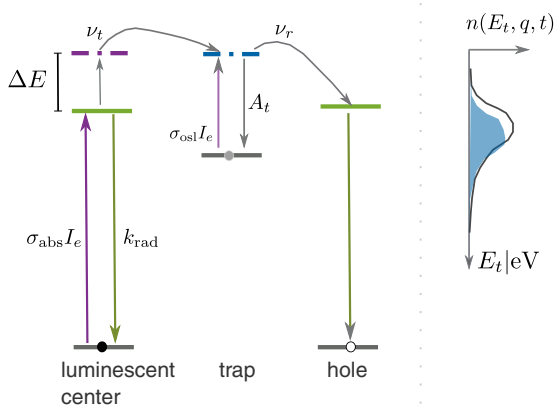
FIG. S4. **Trapping and recombination coefficients**. The elementary "chemical reaction" of trapping and recombination can be described by Eq. S9, and the trapping and recombination coefficients can be approximated by analyzing the relative value of the coefficients depicted in the figure. For the luminescent center, the non-radiative decay coefficient and the stimulated emission cross-section of the excited state have been neglected.

within independent pairs and retrapping has been completely ignored. Here, we consider an elementary event of trapping and recombination. The kinetics of macroscopic densities of the pairs can be described by differential equations by applying the mean-field mass-action law [77]. Hence, the kinetics of elementary events of trapping and recombination can be represented by a chain of mono-molecular "chemical reaction",

$$\text{G} \underset{k_{-1}}{\overset{k_1}{\rightleftarrows}} \text{E} \xrightarrow{k_2} \phi \qquad \text{(S9)}$$
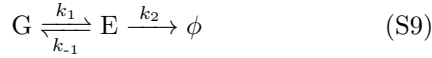
in which G and E represent the ground and excited state, respectively. Herein, ϕ represent the final 'product', which is an electron trapped in traps for trapping and an recombination of electron with hole for recombination, respectively. The density of G and E are often denoted as [G] and [E], respectively. The elementary trapping rate or recombination rate can be written as,

$$R([E]) = k_2[E], \qquad \text{(S10)}$$

in which the meaning of [E] is dependent on the context.

According to Eq. S9, the following differential equations can apply [78],

$$\frac{d}{dt}\begin{bmatrix} [G] \\ [E] \end{bmatrix} = \begin{bmatrix} -k_1 & k_{-1} \\ k_1 & -(k_{-1}+k_2) \end{bmatrix} \begin{bmatrix} [G] \\ [E] \end{bmatrix}. \qquad \text{(S11)}$$

This equation can be solved by matrix methods with initial condition $[G](t=0) = [G]_0, [E](t=0) = 0$ [78],

$$\begin{bmatrix} [G] \\ [E] \end{bmatrix} = \frac{[G]_0}{\lambda_1 - \lambda_2} \begin{bmatrix} k_1 - \lambda_2 & -(k_1 - \lambda_1) \\ -k_1 & k_1 \end{bmatrix} \begin{bmatrix} \exp(-\lambda_1 t) \\ \exp(-\lambda_2 t) \end{bmatrix} \qquad \text{(S12)}$$

in which λ_1 and λ_2 is the eigenvalue of the coefficients matrix in Eq. S11,

$$\lambda_1 = \frac{1}{2}\left[k_1 + k_{-1} + k_2 + \sqrt{(k_1 + k_{-1} + k_2)^2 - 4k_1 k_2} \right] \qquad \text{(S13a)}$$

$$\lambda_2 = \frac{1}{2}\left[k_1 + k_{-1} + k_2 - \sqrt{(k_1 + k_{-1} + k_2)^2 - 4k_1 k_2} \right] \qquad \text{(S13b)}$$

The time for [E] to reach maximum is thus [78],

$$\tau_m = \frac{1}{\lambda_1 - \lambda_2}\ln\left(\frac{\lambda_1}{\lambda_2}\right) \qquad \text{(S14)}$$

and when $t > \tau_m$ it is safe to set $\exp(-\lambda_1 t)$ to zero in Eq. S12, leading to approximated solutions

$$[G] \approx \frac{(\lambda_1 - k_1)[G]_0}{\lambda_1 - \lambda_2}\exp(-\lambda_2 t), \qquad \text{(S15a)}$$

$$[E] \approx \frac{k_1[G]_0}{\lambda_1 - \lambda_2}\exp(-\lambda_2 t). \qquad \text{(S15b)}$$

In the context of TL or PersL, the density $[G] + [E]$ is more convenient. For example, before recombining with a hole, an electron is often reckoned be trapped at either the ground or excited state of the trap, whose density can be described by the electron population function $n(E_t, q, t_c)$. Hence, the following ratio can be calculated easily,

$$r([E]) = \frac{[E]}{[G] + [E]} \approx \frac{k_1}{\lambda_1}. \qquad \text{(S16)}$$

Trapping coefficient. We first consider the case of trapping. The presence of a thermal barrier makes the trapping coefficient to follow the Arrhenius relation with activation energy ΔE. The coefficients for Eq. S9 are

$$k_1 = \sigma_{\text{abs}} I_e(\lambda), \qquad \text{(S17a)}$$

$$k_{-1} = k_{\text{rad}}, \qquad \text{(S17b)}$$

$$k_2 = \nu_t \exp\left(-\frac{\Delta E}{k_{\text{B}} T}\right), \qquad \text{(S17c)}$$

in which stimulated emission of the luminescent center has been neglected because optical excitation in the experiments is weak. It can be seen that,

$$k_{-1} \gg k_1, k_{-1} \gg k_2, \qquad \text{(S18)}$$

which leads to an approximation for $r([E])$,

$$r([E]) \approx \frac{k_1}{k_{-1}} \qquad \text{(S19)}$$

and thus the trapping rate can be calculated by

$$R([E]) = k_2 \times ([G] + [E]) \times r([E]) = \frac{k_1 k_2}{k_{-1}} \times ([G] + [E]). \qquad \text{(S20)}$$

It is quite clear now that the trapping coefficient turns out to be,

$$k_{\text{trap}}(\Delta E, q) = \frac{\nu_t \sigma_{\text{abs}} I_e(\lambda)}{k_{\text{rad}}} \exp\left(-\frac{\Delta E}{k_{\text{B}} T_{ch}}\right), \quad \text{(S21)}$$

which is Eq. 11 in the paper.

Recombination coefficient. The coefficient for an electron in the excited state decay non-radiatively to the ground state of the trap is denoted as A_t. The coefficient for thermal detrapping is $A_t \exp\left(-\frac{E_t}{k_{\text{B}} T}\right)$ for a trap with trap depth E_t. Therefore, the coefficients for the "chemical reaction" Eq. S9 now turns out to be,

$$k_1 = \sigma_{\text{osl}} I_e(\lambda) + A_t \exp\left(-\frac{E_t}{k_{\text{B}} T}\right), \quad \text{(S22a)}$$

$$k_{-1} = A_t, \quad \text{(S22b)}$$

$$k_2 = \nu_r. \quad \text{(S22c)}$$

In this case, the relation holds,

$$k_1 \ll k_{-1}, k_1 \ll k_2. \quad \text{(S23)}$$

which leads to an approximation,

$$r([E]) \approx \frac{k_1}{k_{-1} + k_2}. \quad \text{(S24)}$$

The rate of recombination becomes

$$R([E]) = k_2 \times ([G] + [E]) \times r([E])$$
$$= \frac{k_1 k_2}{k_{-1} + k_2} \times ([G] + [E]), \quad \text{(S25)}$$

which yields the coefficient of recombination,

$$k_{\text{rcb}}(E_t, q) = \frac{A_t}{A_t + \nu_r} \left[\nu_r \exp\left(-\frac{E_t}{k_{\text{B}} T}\right) + \frac{\nu_r}{A_t} \sigma_{\text{osl}} I_e(\lambda) \right], \quad \text{(S26)}$$

which is Eq. 12 in the paper.

V. DOSE DEPENDENCY

The normalized electron population function,

$$n_n(E_t, q, t_c) = \frac{n(E_t, q, t_c)}{\max_{E_t} n(E_t, q, t_c)}$$

reveals the shapes of $n(E_t, q, t_c)$ at different charging condition q. For each charging temperature $T_{ch} = 243, 268, 293, 313,$ and 333 K, the trap depth of the maximum of $n_n(E_t, q, t_c)$, i.e. E_m, shifts to high values with increasing charging duration t_{ch} before reaching its maximum (Fig. S5a). However, the shape of $n_n(E_t, q, t_c)$ stays more or less unchanged with increasing LED current (1-50 mA), with a fixed charging duration $t_{ch} = 30$ s (Fig. S5b). The
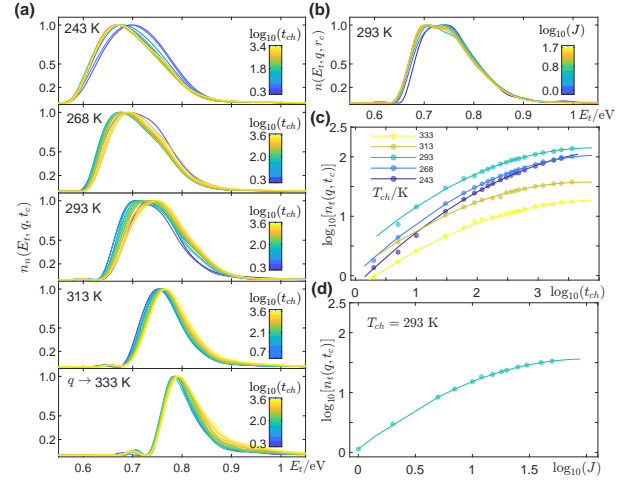

FIG. S5. **Dose dependency**. **(a)** For given various charging temperature T_{ch}, the trap depth of the electron population function maximum E_m increase with increasing chargingduration t_{ch} before reaching its maximum. **(b)** The shape of electron population function does not change greatly with increasing driving current of the LED J = 1-50 mA. **(c)** $\log_{10}[n_t(E_t, q, t_c)]$ is a quadratic function of $\log_{10}(t_{ch})$ for various T_{ch}. **(d)** Similarly, $\log_{10}[n_t(E_t, q, t_c)]$ is also a quadratic function of $\log_{10}(J)$ at $T_{ch} = 293$ K and $t_{ch} = 30$ s. Note the charging temperature T_{ch} is 243, 268, 293, 313, and 333 K in **(a)** and **(c)**.
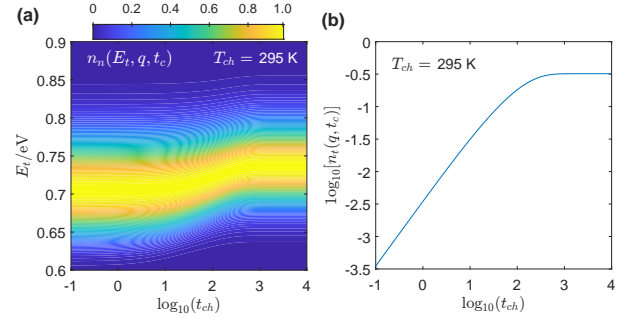

FIG. S6. **Simulation of charging kinetics**. **(a)** The contour plot of $n_n(E_t, q, t_c)$ for various t_{ch} clearly shows that the trap depth of the $n_n(E_t, q, t_c)$ maximum, i.e. E_m, starts shifting to higher value (at $\sim$ 10 s) and reaches stable value for high t_{ch} (at $\sim 10^3$ s). **(b)** The total number of trapped electron per volume $n_t(q, t_c)$ is a function of charging duration t_{ch}, following the formula Eq. S27 when $t_{ch} < 10^3$ s. Note a Gaussian distribution is assumed for $N(E_t)$, i.e. $N(E_t) = \frac{1}{\sqrt{2\pi\sigma^2}} \exp\left[-0.5(E_t - E_u)^2/\sigma^2\right]$, with $E_u = 0.70$ eV and $\sigma = 0.05$ eV.

total number of trapped electrons per volume $n_t(q, t_c)$ is related to the charging duration t_{ch} or driving current of the LED J by a quadratic function in the log-log scale,

$$y = ax^2 + bx + c \quad \text{(S27)}$$

in which $y = \log_{10}[n_t(q, t_c)]$, $x = \log_{10}(t_{ch})$ or $x = \log_{10}(J)$ (Fig. S5c-d).

To understand these observations, a simulation of elec-

tron population has been performed for a Gaussian distribution of trap depth,

$$N(E_t) = \frac{1}{\sqrt{2\pi\sigma^2}}\exp\left[-\frac{(E_t - E_u)^2}{2\sigma^2}\right],$$

with $E_u = 0.70$ eV and $\sigma = 0.05$ eV. This distribution agrees with the one obtained in the paper. The simulation of $n_n(E_t, q, t_c)$ reveals that E_m increases almost linearly with increasing $\log_{10}(t_{ch})$ (Fig. S6a). In addition, the simulated $\log_{10}[n_t(q, t_c)]$ can be related to $\log_{10}(t_{ch})$ by a quadratic function when $t_{ch} <\sim 10^3$ s (Fig. S6b). It is interesting to note that the change of the position of the electron population with increasing charging duration can be explained by a first-order kinetics for a trap depth distribution rather than non-first order kinetics.

Herein, we provide the MATLAB code for the simulation.

```
1 • % the initialization
2   kB = 0.08617; % meV/K
3   nu_r = 1e10; nu_t = nu_r; A_t = 1e12;
4   sigma_osl = 1e-17; sigma_abs = 3e-18; %
        cross-sections
5   krad = 1.54e6; % radiative rate of Eu
        in BaSiON, Hz
6   dE = 255; Ie_exp = 5e15; beta = 0.5;
7
8   syms deltaE Ie t T Et Ti
9   ktrap = @(deltaE,T,Ie) 1*nu_t*exp(-
        deltaE./(kB*T))*sigma_abs.*Ie/krad;
10  krcb = @(Et,T,Ie) (nu_r*exp(-Et./(kB*T)
        )+sigma_osl.*Ie*nu_r/A_t)/(1+nu_r/
        A_t);
11  filling = @(Et,deltaE,T,Ie,t) ktrap(
        deltaE,T,Ie)./(ktrap(deltaE,T,Ie)+
        krcb(Et,T,Ie)).*(1-exp(-(ktrap(
        deltaE,T,Ie)+krcb(Et,T,Ie)).*t));
12  % the above is the filling function
13  tInt = @(Et,T) 0.25*kB*nu_r/beta*(T
        .^2./Et).*exp(-Et./T/kB)./sqrt(1+4*
        kB*T./Et); % effective cooling/
        heating rate is 4beta
14  TempInt = @(Et,T) tInt(Et,T)-tInt(Et,T
        -30); % cooling down to T0 = T-30 K
15  cool = @(Et,T) exp(-TempInt(Et,T));
16  tch = logspace(-3.0,4,200)'; % tch in
        log10 space
17  dE = 1; Ea = 50; Eb = 2e3; E = (Ea:dE:
        Eb)'; % meV
18  [tgrd,Egrd] = meshgrid(tch,E);
19  Tch = 295; % charging temperature
20  Fill = filling(Egrd,dE,Tch,Ie_exp,tgrd)
        ;
21  Fillcool = Fill.*cool(Egrd,Tch);
22  % calculate gaussian distribution
23  Eav = 700; Estd = 50; %
24  NE = 1/sqrt(2*pi*Estd^2)*exp(-0.5*(E-
        Eav).^2./Estd^2); % gaussian
        distribution;
```

```
25  Nn = (NE.*Fillcool)./max(NE.*Fillcool
        ,[],1);% normalized electron
        population function
26  lgnt = log(sum(NE.*Fillcool)*dE)/log
        (10); % n_t in log10 scale
```

After the simulation, Fig. S6 can be generated easily.

VI. SIMPLIFICATION OF THE KERNEL

The temperature integral $F(E_t, T_0)$ should be significantly smaller than $F(E_t, T)$ when T_0 is about ~ 30 K smaller than T. This further leads to an approximated kernel, which is Eq. 24 in the paper. Furthermore, the decay profile of persistent luminescence can be analyzed by the Fredholm integral with the kernel Eq. 29 in the paper. The details of the derivation will be given in the following.

At a given temperature $T > T_0 + 20 \sim 30$ K, the kernel $K(E_t, T)$ can be approximated by neglecting $F(E_t, T_0)$,

$$K(E_t, T) = \exp\left[-\frac{E_t}{k_B T} - F(E_t, T)\right]. \tag{S28}$$

The derivative of $\ln[K(E_t, T)]$ with respect to E_t is,

$$\frac{\partial}{\partial E_t}\ln[K(E_t, T)] = -\frac{1}{k_B T} + \frac{\nu_r}{\beta}\int_0^T \frac{1}{k_B T'}\exp\left(-\frac{E_t}{k_B T'}\right)dT'. \tag{S29}$$

After following substitution,

$$t = \frac{E_t}{k_B T'}, \qquad x = \frac{E_t}{k_B T},$$

the second term in Eq. S29 can be simplified as,

$$\frac{\nu_r}{\beta}\int_0^T \frac{1}{k_B T'}\exp\left(-\frac{E_t}{k_B T'}\right)dT' = \frac{\nu_r}{k_B\beta}\int_x^\infty \frac{\exp(-t)}{t}dt$$
$$= \frac{\nu_r}{k_B\beta}E_1(x),$$

where the exponential integral $E_1(x)$ can be approximated by [79],

$$E_1(x) = \frac{\exp(-x)}{x + 1}. \tag{S30}$$

Setting Eq. S29 to zero means,

$$-\frac{1}{k_B T} + \frac{\nu_r}{k_B\beta}\frac{\exp(-x)}{x + 1} = 0, \tag{S31}$$

which leads to the root,

$$x_s = W(e\nu_r T/\beta) - 1 \tag{S32}$$

where e $= \exp(1)$ and $W(x)$ is the Lambert W function with branch $n = 0$. This results in Eq. 25b in section IVA of the paper,

$$E_s(T) = k_\mathrm{B}T\left[W(\mathrm{e}\nu_r T/\beta) - 1\right].$$
(S33)

According to Eq. S31, the following holds,

$$\exp(-x_s) = \frac{\beta(x_s + 1)}{\nu_r T},$$

which further leads to,

$$\exp\left(-\frac{E_s}{k_\mathrm{B}T}\right)\frac{\nu_r}{\beta}\frac{k_\mathrm{B}T^2}{E_t} = \frac{E_s + k_\mathrm{B}T}{E_t}$$
(S34)

The kernel Eq. S28 was initially expressed as

$$K(E_t, E_s) = \frac{\nu_r}{\beta}\exp\left(-\frac{E_s}{k_\mathrm{B}T}\right)\exp\left[-\frac{E_t - E_s}{k_\mathrm{B}T}\right. $$
$$- \exp\left(-\frac{E_t - E_s}{k_\mathrm{B}T}\right)\exp\left(-\frac{E_s}{k_\mathrm{B}T}\right) $$
(S35)
$$\times \left.\frac{\nu_r}{\beta}\frac{k_\mathrm{B}T^2}{E_t}\frac{1}{\sqrt{1 + 4k_\mathrm{B}T/E_t}}\right]$$

which results in Eq. 25a immediately by utilizing Eq. S34. The magnitude of the kernel Eq.S35 is,

$$\boxed{\frac{\nu_r}{\beta}\exp\left(-\frac{E_s}{k_\mathrm{B}T}\right) = W(\mathrm{e}\nu_r T/\beta)/T}$$
(S36)

which changes with T at the rate of

$$\frac{\partial}{\partial T}\frac{\nu_r}{\beta}\exp\left(-\frac{E_s}{k_\mathrm{B}T}\right) = -\frac{W(\mathrm{e}\nu_r T/\beta)}{T^2}\frac{W(\mathrm{e}\nu_r T/\beta)}{W(\mathrm{e}\nu_r T/\beta) + 1}.$$
(S37)

The derivative of E_s with respect to T is

$$\frac{\partial E_s}{\partial T} = k_\mathrm{B}W(\mathrm{e}\nu_r T/\beta)\frac{W(\mathrm{e}\nu_r T/\beta) + 2}{W(\mathrm{e}\nu_r T/\beta) + 1} - k_\mathrm{B}$$
(S38)

Similarly, the decay profile of persistent luminescence can be given in the following integral equation,

$$I(t_0) = \int_0^\infty K(E_t, t_0)n(E_t, q, t = 0)dE_t$$
(S39)

in which the kernel reads,

$$K(E_t, t_0) = \nu_r\exp\left(-\frac{E_t}{k_\mathrm{B}T}\right)\exp\left[-\int_0^{t_0}\nu_r\exp\left(-\frac{E_t}{k_\mathrm{B}T}\right)dt\right].$$
(S40)

It can be rewritten in the form,

$$K(E_t, t_0) = \nu_r\exp\left(-\frac{E_s(t_0)}{k_\mathrm{B}T}\right)\times$$
$$\exp\left[-\frac{E_t - E_s(t_0)}{k_\mathrm{B}T}\right.$$
$$\left.- \exp\left(-\frac{E_t - E_s(t_0)}{k_\mathrm{B}T}\right)\times \nu_r t_0\exp\left(-\frac{E_s(t_0)}{k_\mathrm{B}T}\right)\right],$$

from which the characteristic trap depth $E_s(t_0)$ can be found by seeking the root of

$$\nu_r t_0\exp\left(-\frac{E_s(t_0)}{k_\mathrm{B}T}\right) - 1 = 0$$

leading to

$$\boxed{E_s(t_0) = k_\mathrm{B}T\ln(\nu_r t_0)},$$
(S41)

which is Eq. 28b in the paper. The magnitude of the kernel $K(E_t, t_0)$ is,

$$\nu_r\exp\left(-\frac{E_s(t_0)}{k_\mathrm{B}T}\right) = \frac{1}{t_0}$$

and thus the kernel can be written in the compact form,

$$\boxed{K(E_t, t_0) = \frac{1}{t_0}\exp\left[-\frac{E_t - E_s(t_0)}{k_\mathrm{B}T} - \exp\left(-\frac{E_t - E_s(t_0)}{k_\mathrm{B}T}\right)\right]},$$
(S42)

which is Eq. 28a in the paper.